Photon Factory Activity Report 2001 #19B
–Users' Report–

▶ *Atomic and Molecular Science*
▶ *Applied Science*
▶ *Biological Science*
▶ *Chemistry*
▶ *Crystallography*
▶ *Electronic Structure of Condensed Matter*
▶ *High Pressure Science*
▶ *Instrumentation and Technique*
▶ *Medical Applications*
▶ *Materials Science*
▼ ***Surface and Interface***

193 X-ray magnetic circular dichroism study on spin reorientation transitions of Co/Pd(111) induced by surface chemisorption
Isao TAKAHASHI, Kouji INOUE, Hiroyuki KIKKAWA, Kyohiko MATSUSHITA, Amane KITAHARA
7A/1999G159

194 X-ray reflectivity of a polystyrene surface peeled from a Si(100) mold: Morphology and surface glass transition
Isao TAKAHASHI, Kouji INOUE, Hiroyuki KIKKAWA, Kyohiko MATSUSHITA, Amane KITAHARA
4C,17A/2000G053

195 Study of a-Si/1ML-Ge/Si(001) interface structure by X-ray standing wave
Shinichiro NAKATANI, Kazushi SUMITANI, Akinobu NOJIMA, Toshio TAKAHASHI, Keiichi HIRANO, Shinji KOH, Toshifumi IRISAWA, Yasuhiro SHIRAKI
14B,15C/2000G056

196 The kinetic study for fat crystallization process in O/W emulsion
Satoru UENO, Yoshito HAMADA, Yoshiyuki AMEMIYA, Kiyotaka SATO
15A,9C/2000G067

197 Quasi-amorphous structure in the thermal oxide layer on an Si(113) substrate
Takayoshi SHIMURA, Takayoshi YOSHIDA, Kiyoshi YASUTAKE
4C,17A,18B/2000G101

198 EXAFS studies on the MCM-41 supported NbC catalysts
Nobuyuki ICHIKUNI, Hirohisa HACHIYA, Shogo SHIMAZU, Takayoshi UEMATSU
10B/2000G111

199 Magnetic domain imaging of Ni micro-dot array by photoelectron emission microscope(PEEM)
Taichi OKUDA, Takanori WAKITA, Ayumi HARASAWA, Hideyuki KIWATA, Takeshi MATSUSHIMA, Takayuki KIHARA, Kanta ONO, Masaharu OSHIMA, Atsushi YOKOO, Toyohiko KINOSHITA
11A/2000G171

200 Magnetic domain structure of Ni micro-ring observed by photoelectron emission microscope (PEEM)
Taichi OKUDA, Takanori WAKITA, Ayumi HARASAWA, Hideyuki KIWATA, Takeshi MATSUSHIMA, Kanta ONO, Atsushi YOKOO, Masaharu OSHIMA, Toyohiko KINOSHITA
11A/2000G171

201 Study of Ni/4H-SiC contact by using soft X-ray florescence spectroscopy
Masaaki HIRAI, Akihiko OHI, Joselito P. LABIS, Chihiro KAMEZAWA, Kenichi YOSHIDA, Masahiko KUSAKA, Motohiro IWAMI
19B/2000G181

202 Strain due to Ni diffusion beneath Hydrogen-terminated Si(111) surface
Takashi EMOTO, Koichi AKIMOTO, Ayahiko ICHIMIYA, Kazuyuki HIROSE
15C/2000G200

203 In-situ XAFS study of Ag clusters in zeolite 13X
Takafumi MIYANAGA, Yushi SUZUKI, Hideoki HOSHINO, Naoyuki MATSUMOTO, Takeshi AINAI
10B/2000G272

204 Polarization dependent total reflection fluorescence XAFS(PTRF-XAFS) studies on Ni atoms dispersed on Al_2O_3(0001) surface
Kaoru IJIMA, Yuichiro KOIKE, Kiyotaka ASAKURA, Yasuhiro TANIZAWA, Takafumi SHIDO, Yasuhiro IWASAWA
9A/2000G276

205 Formation process of β-$FeSi_2$ on Si (111) substrate studied by means of SR-XPS
Takeru SAITO, Hiroyuki YAMAMOTO, Masaharu HARAGUCHI, Motoyasu IMAMURA, Nobuyuki MATSUBAYASHI, Tomoaki TANAKA, Hiromichi SHIMADA, Kiichi HOJOU
13C/2000G280

206 In-situ XAFS observation of USY supported Pd-Pt catalysts during sulfidation process
Kyoko K. BANDO, Takashi MATSUI, Lionel LE BIHAN, Koichi SATO, Tomoaki TANAKA, Motoyasu IMAMURA, Nobuyuki MATSUBAYASHI, Yuji YOSHIMURA
9A,10B/2000G283

207 *In-situ* XAFS characterization of Mo/SiO_2 catalyst during propene photometathesis reaction
Haruno MURAYAMA, Nobuyuki ICHIKUNI, Kyoko K. BANDO, Shogo SHIMAZU, Takayoshi UEMATSU
10B/2000G286

208 Crystal orientation of silver films on silicon surfaces
Atsushi HATA, Koichi AKIMOTO, Shinji HORII, Takashi EMOTO, Ayahiko ICHIMIYA, Hiroo TAJIRI, Toshio TAKAHASHI, Hiroshi SUGIYAMA, Xiaowei ZHANG, Hiroshi KAWATA
15B2/2000S2-003

209 Temperature dependence of the Si(111)-$\sqrt{3}\times\sqrt{3}$-Ag structure
Hiroo TAJIRI, Kazushi SUMITANI, Toshio TAKAHASHI, Koichi AKIMOTO, Hiroshi SUGIYAMA, Xiaowei ZHANG, Hiroshi KAWATA
15B2/2000S2-003

210 Chemical structure of the SiO_2/Si(001) interface formed at high temperatures
Hiroo OMI, Satoru SUZUKI, Yoshio WATANABE, Toshio OGINO
1C/2001C009

211 P and S K-edge XANES measurements of tribofilms formed on steel disks in conversion electron yield and fluorescence yield modes
Yoshimu IWANAMI, Toru MAKISHIMA, Takaki OKUBO, Masaharu NOMURA
9A/2001C014

212 Depth-resolved XMCD study on Fe/Cu(001)
Soichiro KITAGAWA, Kenta AMEMIYA, Daiju MATSUMURA, Toshihiko YOKOYAMA, Toshiaki OHTA
7A/2001G013

213 Si L_{23} emission spectra from the interfaces in antiferromagnetically coupled Fe/Si multilayers II
Takashi IMAZONO, Yushi HIRAYAMA, Noboru MIYATA, Osamu KITAKAMI, Mihiro YANAGIHARA
3B,16B/2001G021

214 Grading effects in X-ray specular reflectivity analysis
Mari MIZUSAWA, Kenji SAKURAI
14A/2001G045

215 Grazing-incidence diffuse scattering for Ni/C multilayers
Shuichiro KUWAJIMA, Hisataka TAKENAKA, Kenji SAKURAI
14A/2001G045

216 Grazing-incidence X-ray specular reflectivity study on a rutile (110) surface
Mari MIZUSAWA, Kenji SAKURAI
14A/2001G045

217 Study of α-Al_2O_3/Ru(0001) structure by X-ray diffraction
Shinichiro NAKATANI, Toshio TAKAHASHI, Kazuo NAGATA, Wataru YASHIRO, Yoshitada MURATA
9C,14B,15C/2001G055

218 Characterization of a-Si/Fe/Si(111) interface by X-ray standing wave
Shinichiro NAKATANI, Keisuke SHIMIZU, Toshio TAKAHASHI, Keiichi HIRANO
9C,14B,15C/2001G065

219 Carbon K-edge x-ray absorption spectroscopic analysis of photo-degraded polyimide film
Tomoaki TANAKA, Kyoko K. BANDO, Nobuyuki MATSUBAYASHI, Motoyasu IMAMURA, Hiromichi SHIMADA
13C/2001G108

220 Anomalous redox properties of copper-ion-exchanged ZSM-5 prepared by microwave-assisted method
Takae OKAMOTO, Atsushi ITADANI, Ryotaro KUMASHIRO, Masatoshi MARUKI, Hideo ONISHI, Yasushige KURODA, Yuzo YOSHIKAWA, Mahiko NAGAO
10B/2001G128

221 Surface chemical imaging of energy filtered photoemission electron microscopy(EXPEEM)
Hideyuki YASUFUKU, Yusuke OHMINAMI, Tetsuya TSUTSUMI, Kiyotaka ASAKURA, Yoshiyuki KITAJIMA, Makoto KATO, Yuji SAKAI, Yasuhiro IWASAWA
11B/2001G312

222 Core level spectroscopy study for cluster-like Si deposited on graphite and insulating sapphire
Krishna G. NATH, Iwao SHIMOYAMA, Tetsuhiro SEKIGUCHI, Yuji BABA
27A/2001G334

223 XPS and NEXAFS observations on Si_xC produced by ion implantation
Yuji BABA, Iwao SHIMOYAMA, Tetsuhiro SEKIGUCHI, Krishna G. NATH
27A/2001G334

224 Metal induced gap states at LiCl/Cu(001) interface studied by x-ray absorption fine structure
Manabu KIGUCHI, Genki YOSHIKAWA, Masao KATAYAMA, Koichiro SAIKI, Atsushi KOMA
11B/2001G336

225 Structures of low-dimensional ionic solutions confined in solid nanospaces
Takahiro OHKUBO, Yoshiyuki HATTORI, Hirofumi KANOH, Katsumi KANEKO
10B/2001P016

226 In-situ observation of water formation reaction on Pt(111) with dispersive NEXAFS
Masanari NAGASAKA, Hiroshi KONDOH, Kenta AMEMIYA, Akira NAMBU, Toru SHIMADA, Ikuyo NAKAI, Toshiaki OHTA
7A/2001S2-003

227 The mechanism of CO oxidation on Pt(111) surface studied by energy-dispersive NEXAFS
Ikuyo NAKAI, Hiroshi KONDOH, Kenta AMEMIYA, Akira NAMBU, Toru SHIMADA, Masanari NAGASAKA, Toshiaki OHTA
7A/2001S2-003

7A/1999G159

X-ray magnetic circular dichroism study on spin reorientation transitions of Co/Pd(111) induced by surface chemisorption

Daiju MATSUMURA*[1], Toshihiko YOKOYAMA[2], Kenta AMEMIYA[1], Soichiro KITAGAWA[1], Norihiro SUZUKI[1], Toshiaki OHTA[1]
[1] The University of Tokyo, 7-3-1 Hongo, Bunkyo-ku, Tokyo 113-0033, Japan
[2] Institute for Molecular Science, Myodaiji-cho, Okazaki, Aichi 444-8585, Japan

Introduction

The perpendicular magnetic anisotropy (PMA) of ultrathin films has been investigated widely because PMA is energetically unstable if one considers only classical magnetic dipole-dipole interaction. Recently, it is reported that H or CO surface chemisorption stabilizes PMA of Ni/Cu(001) by using Kerr effect [1]. We have revealed that H and CO adsorption stabilize PMA of Ni/Cu(001) in different mechanism that depends on surface adsorption fashion by using x-ray magnetic circular dichroism (XMCD). And we have investigated surface adsorption effects of Co/Pd(111) by means of XMCD and discovered that CO or NO surface chemisorption stabilizes PMA [2]. In the case of CO adsorption, from the viewpoint of surface orbital magnetic moment, it is revealed that anisotropic change of surface orbital moment induced by CO chemisorption is the key of stabilization of PMA and the anisotropic change is attributed to the surface chemisorption fashion.

Experiments

XMCD study was taken at the bending-magnet station Beamline BL-7A. All the experiments were performed in a UHV atmosphere. A single crystal of Pd(111) was cleaned by the cycles of Ar^+ sputtering (2 kV) and subsequent annealing at 1070 K. Co was evaporated by electron-bean evaporation method. The thickness of films was calibrated by Auger intensity ratio between Co and Pd.

Circularly polarized x rays were obtained by using upper or lower ($\pm$0.4 mrad) part from the storage ring. The circular polarization factor is about 80 %. All the spectra were recorded in a partial-electron-yield mode by using microchannel plate with retarding voltage of -500 V. The films were magnetized by a current pulse. The XMCD spectra were obtained by reversing the magnetization of films. The remanent magnetization was examined.

Results

We performed normal (90 deg.) and grazing (30 deg.) incidence study to know the easy axis of the films. The critical thickness is about 3.5 ML in the case of surface clean films. Below the critical thickness, films have perpendicular magnetization and above that films have parallel one. On the other hand, CO-covered films have larger perpendicular magnetization region. CO adsorption spread the perpendicular magnetization region about 3 ML.

Fig. 1 shows orbital magnetic moment before and after CO adsorption. From the viewpoint of magnetic easy axis, we classify Co thickness into three regions. In region I, the films have always perpendicular magnetic moment even before CO adsorption and perpendicular orbital moment is almost conserved. In region III, the films have always parallel magnetic moment even after CO adsorption and parallel orbital moment is quenched by CO adsorption. In region II, spin reorientation transition from parallel to perpendicular occurs and perpendicular orbital moment (after CO adsorption) is larger than parallel (before CO adsorption) one. The anisotropic change of the surface orbital moment is the main issue of PMA stabilization by surface chemisorption.

Different type in changing of orbital moment is attributed to CO adsorption fashion. CO adsorbs on surface with keeping molecular axis almost perpendicular and only parallel orbital moment is quenched.

References

[1] R. Vollmer et al., Phys. Rev. B 60, 6277 (1999).
[2] D. Matsumura et al., Phys. Rev. B 66, 024402 (2002).

* daiju@chem.s.u-tokyo.ac.jp

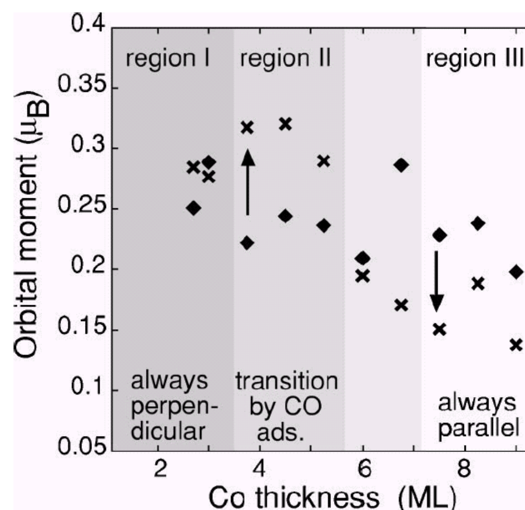

Fig. 1. Orbital magnetic moments of the Co films on Pd(111) at 200 K as a function of Co thickness. Diamonds and crosses denote clean and CO-adsorbed Co, respectively.

4C, 17A/2000G053

X-ray reflectivity of a polystyrene surface peeled from a Si(100) mold: Morphology and surface glass transition

Isao TAKAHASHI*, Kouji INOUE, Hiroyuki KIKKAWA, Kyohiko MATSUSHITA, and Amane KITAHARA

School of Science and Technology, Advanced Research Center of Science, Kwansei Gakuin University (ARCS-KGU), Sanda 669-1337, Japan

Introduction

X-ray diffraction is known to be a powerful tool for non-destructive studies of surface structures. Especially, with the usage of intense synchrotron radiation sources, X-ray reflectivity (XR) has been dedicated to investigate surface structures and morphology of non-crystalline materials under various conditions [1, 2].

Surface and interface of polymers is attracting a great interest due to its potential ability for electronic devices in near future, and of course, due to scientific interest in statistical physics of two-dimensional complex systems. However, lots of the polymer surfaces studied so far have been prepared by the so-called spin-cast method in which unexpected, nuisance effects of the solvent and those from the highly confined geometry of the thin polymer layers, being sometimes comparable with the polymers' gyration radius are inevitable. We would like to observe a solvent-free surface of a polymer sample with macroscopic thickness, which is prepared by a novel method, so as to study the surface glass transitions more naturally. In the present study, we tried to measure the XR from a flat polymer surface with elevating temperatures so as to study glass transitions at polymer surfaces.

Experimental

A flat polystyrene (PS) surface was obtained as follows: (1) a lump of melted PS (M_w=310000, bulk glass transition temperature T_g(bulk)=370K) was dropped onto a polished silicon wafer; (2) annealed up to 450K for six hours and quenched down to the room temperature; (3) the PS of which dimension was 20mm*20mm*2mm was peeled from the flat silicon wafer at room temperature. The measurements were performed by using high resolution four-circle diffractomators installed at BL4C and at BL17A; the wavelengths were chosen to be 1.54 Angstrom and 1.3Angstrom, respectively. Dimension of the incident X-ray was about 0.1mm×1.0mm at the sample position. The PS sample was mounted on a home made oven of which temperature was controlled by a PID unit within 0.5K ranging from the room temperature to 400K.

Results and Discussion

The observed XR revealed the density profile along the surface normal direction; it indicated a fairly flat surface with the root mean square roughness of 1nm. X-ray diffuse Reflectivity showed the non-fractal height-height surface correlation at room temperature; it appeared that the interface between the PS and the Si was formed after condensation of capillary wave fluctuations.

The XR changed drastically with the heating process indicating the considerable variation in electron density at the surface, although the X-ray diffraction from the bulk PS showed no variation. Consequently, the surface glass transition temperature T_g(surface) of the sample was estimated to be 50K lower than that of T_g(bulk). On the other hand, a surface of PS which was fully placed at room temperature for a long time (more than 14 days) did not show such complex variation observed in this study. Present results should be discussed on a standpoint of conformation of polymers. Furthermore, such a large difference between T_g(surface) and T_g(bulk) can be compared with that between the surface melting temperature and bulk melting temperature for ordinary crystals.

References

[1] M. Tolan, *X-ray Scattering from Soft-Matter Thin Films*, Springer, Berlin Heidelberg, 1999.

[2] R. J. Roe, p236 in *Methods of X-ray and Neutron Scattering in Polymer Science*, Oxford Univ. Press, Oxford, 2000.

*suikyo@ksc.kwansei.ac.jp

14B, 15C/2000G056

Study of a-Si/1ML-Ge/Si(001) interface structure by X-ray standing wave

Shinichiro NAKATANI*[1], Kazushi SUMITANI[1], Akinobu NOJIMA[1], Toshio TAKAHASHI[1], Keiichi HIRANO[2], Shinji KOH[3], Toshifumi IRISAWA[3] and Yasuhiro SHIRAKI[3]
[1]Institute for Solid State Physics, The University of Tokyo
Kashiwanoha, Kashiwa, Chiba 277-8581, Japan
[2]Institute of Materials Structure Science, KEK-PF, High Energy Accelerator Research Organization
Oho-machi, Tukuba, Ibaraki 305-0801, Japan
[3]Department of Applied Physics, School of Engineering, The University of Tokyo Bunkyo-ku, Tokyo 113-8656, Japan

Introduction

Very fine structures at the hetero-interface have been realized by the recent development of molecular beam epitaxy (MBE). Exact characterizations for those structures are necessary to fabricate new devices using them. X-rays are useful for the characterization because they can investigate buried interfaces without destroying the structures. Especially, X-ray standing wave (XSW) is a unique method for its fine spatial resolution since it makes use of the interference fringes of x-rays as a scale. We examined the interface structure of an a-Si/Ge/Si(001) crystal by XSW. Besides the view point of fundamental science, this system is interesting from the viewpoint of application; the SiGe-based hetero-structures have a possibility for novel devices like ultra fast LSI and optoelectronic devices.

Experimental

Our sample was prepared by the MBE deposition of 1ML of Ge on the Si(001) substrate followed by the MBE deposition of 1ML of Si and the subsequent deposition of an a-Si cap layer of 50 Å to stabilize the Ge-interface structure.

The experiment was performed using synchrotron radiation from a vertical wiggler of BL-14B. X-rays of wavelength 1 Å were selected by a double-crystal monochromator. The X-rays were reflected by a Si(111) fore crystal and incident on the sample. The skew 111 reflection of the Si(001) substrate was used so that the (+,-) parallel setting was completed.

The intensity curve of the X-rays reflected from the sample (rocking curve) and the yield curve of fluorescent X-rays of GeKα were measured around the 111 Bragg point in the skew arrangement.

Results and discussion

The result of the measurement is shown in Fig.1. The profile of the measured rocking curve is slightly different from calculation at both tails. This means that the strain in the substrate is not negligible. The fluorescence yield curve, which indicates the interaction between the XSW field and Ge atoms, shows that the most of Ge atoms stay 0.7 Å below the ideal Si site. This result is different from other reports[1,2] probably because of the effect of the strain.

In the last machine time of this project, we performed the same measurement under the stress free condition. The result of data analysis will be reported elsewhere[3].

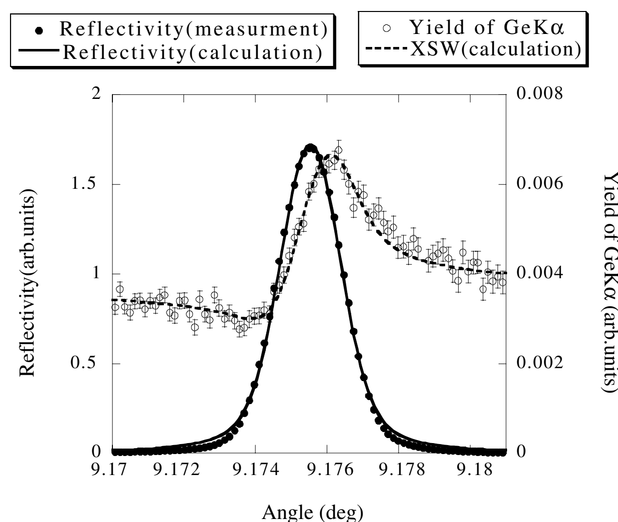

Fig.1. Rocking curve of the 111 reflection and yield of GeKα fluorescence.

References

[1] M.Takahasi et al., Jpn. J. Appl. Phys. **34** 2278 (1995).
[2] J. Falta et al., Surf. Rev. Let. **5**, 145 (1998).
[3] S. Nakatani et al., submitted to ISCSI-4.

*nakatani@issp.u-tokyo.ac.jp

9C, 15A/2000G067

The kinetic study for fat crystallization process in O/W emulsion

Satoru UENO*[1], Yoshito HAMADA[1], Yoshiyuki AMEMIYA[2], Kiyotaka SATO[1]
[1]Hiroshima Univ., Higashi-Hiroshima 739-8528, Japan
[2]The Univ. of Tokyo, Hongo, Bunkyo-ku, Tokyo 113-0001, Japan

Introduction

Crystallization of oil phase in oil-in-water (O/W) emulsion is an important process for coagulation of the emulsions at chilled states, demulsifying process of whipping creams, freezing of ice creams, etc.

Many studies have recently been performed on clarification of the fat crystallization process in the O/W emulsion, whose complexity may be revealed in the rate and extent of crystallization of fats, polymorphism, effects of emusifiers on the crystallization, influences of emulsion droplet sizes, effects of rate of cooling and subsequent temperature history on the physical properties of fats, etc [1, 2].

Revealing the crystallization mechanisms in this system, we studied a model O/W emulsion system of even-carbon number alkan such as n-hexadecane(C_{16}) as oil phase by time-resolved X-ray diffraction.

Materials and methods

Materials: Even-carbon number alkan, from C_{12} to C_{22}, and Tween 20 (polyoxysorbitan monolaurate) were used as oil phase and emulsifier, respectively. Sucrose oligoesters (SOEs), polyglycerol polyesters (PGEs) and diacylglycerols, whose concentrations were 1 wt% and 0.2 wt% for oil phase, were added in oil phase as additives for promoting crystallization of oil phase.

Methods: SAXS-WAXS-DSC simultaneous measurement was performed at BL-15A and BL-9C. Data for X-ray diffraction were detected in every 10 sec. DSC was operated on the cooling and following heating between 25 °C and –10 °C with ±2 °C/min.

Results and Discussion

We, here, mainly report the results of the system of n-hexadecane in oil phase. As for the other alkans, the same kinds of results of n-hexadecane were observed.

O/W emulsion without additives:

When the DSC exothermic and endothermic peaks, which corresponded to the crystallization and melting of n-hexadecane, appeared at 2.0 °C and 19.4 °C, respectively, the XRD peaks, at 2.09, 0.46, 0.45, 0.40, 0.38, 0.36 nm, also appeared and disappeared. This suggest that all of the diffraction peaks correspond the crystallization and melting of n-hexadecane.

O/W emulsion with additives:

In the cooling process, when the first exothermic DSC peak appeared at 7.7 °C, the 2.2, 0.42, 0.38 nm diffraction peaks, which did not appeared in the non-additive system, appeared. In the following, the diffraction peaks which corresponded those of n-hexadecane mentioned the previous paragraph appeared when the second DSC peak appeared at 5.5 °C. When the third DSC peak appeared at -4.3 °C, the diffraction peak at 0.42 nm suddenly shifted to 0.41 nm. In the heating process, 0.41 nm suddenly shifted to 0.42 nm corresponding to the DSC endothermic peak at 4.3 °C. The diffraction peaks at 2.2 and 0.42 nm disappeared corresponding to the DSC endothermic peak at 16.6 °C. Finally, when the DSC endothermic peak appeared at 19.4 °C, the rest diffraction peaks which were corresponded to those of n-hexadecane disappeared.

Since those peaks at 2.2, 0.42, 0.38 nm appeared neither in the mixed bulk system nor in the non-additive O/W emulsion system, we thought as follows; (1) these peaks indicated the existence of a complex crystal whose period of lamellar and lateral packings are 2.2 nm, and 0.42 and 0.38 nm, respectively, (2) this complex existed on the surface between water and oil droplet, (3) the melting and crystallization temperature of this complex were 16.6 and 7.7 °C, respectively. The lowest DSC peak corresponded to the transformation of this complex at 4.3 °C in heating and -4.3 °C in cooling process, (4) as for crystallization of n-hexadecane, at first, the complex structure forms, and, secondly, the crystallization of the n-hexadecane occurs; namely, the complex works a kind of template for crystallization of the oil phase.

After additional SAXS-WAXS-DSC simultaneous experiment for O/W emultion using odd-number alkan, pentadecane(C15), heptadecane(C17), nonadecane(C19), as oil phase, it was revealed that the "complex" was the crystal of orthorhombic form for even-number alkan; the same WAXS diffraction peaks, 0.42 and 0.38 nm, and shift from 0.42 to 0.41 nm appeared in odd-number alkan O/W emulsions. While even-number alkan normally forms triclinic polymorph in bulk system, odd-number alkan forms orthorhombic one.

In conclusion, at first, a special orthorhombic crystal for even-number alkan was crystallized along the oil-water interface consist of emulsifier and additives, and, secondly, this crystal worked as a kind of template for crystallizing the next normal triclinic polymorph of oil phase.

References

[1] E. Dickinson et al., in Advances in Food Colloids, Blackie Academic & Professional, London, pp.247 (1995).
[2]S. Hindle et al., J.Colloid.Interface Sci. 232,370 (2000).

* sueno@hiroshima-u.ac.jp

4C, 17A,18B/2000G101

Quasi-amorphous structure in the thermal oxide layer on an Si(113) substrate

Takayoshi SHIMURA, Takayoshi YOSHIDA, and Kiyoshi YASUTAKE
Osaka Univ., 2-1 Yamadaoka, Suita, Osaka 565-0871, Japan

Introduction

In the X-ray diffraction patterns from thermal oxide thin films on Si(001), (111), and (110) wafers, very weak diffraction peaks are observed on the low angle side of the crystal truncation rod (CTR) scattering around the 111 Bragg points. The intensity of the extra peak depends on the thickness of the oxide layer and is not observed from the sample when the oxide layer is removed by etching in HF solution. The intensity profile along the CTR scattering shows the Laue-function-like oscillation pattern near the extra peak, of which period corresponds to the inverse of the film thickness. The angular width of the peak perpendicular to the CTR scattering is the same order of magnitude as that of the CTR scattering from the substrate. From these results we speculated that the thermal oxide layer has quasi-amorphous structure, in which the atoms were displaced from the average positions, but the average lattice has epitaxial relation with the substrate [1-5].

In this study we examined the existence of the ordered structure in the thermal oxide layer on a Si(113) wafer, which may be a competitive substrate material for Si integrated circuits [6].

Experimental

A Si(113) wafer was oxidized in dry O_2 ambient at 850 °C. The thickness of the oxide layer is about 23nm.

X-ray diffraction patterns using an imaging plate (IP) detector were obtained with a Weissenberg camera at BL-18B. X-rays with the wavelength of 0.1nm were employed. For quantitative measurements, the four-circle diffractometer with a Si(111) crystal analyzer installed on BL-4C was used. The measurements were carried out at the symmetric condition using X-rays with the wavelength of 0.1542 nm.

Results

The intensity distribution of the CTR scattering elongated from the 111 Bragg point is shown in Fig.1(a). The horizontal axis indicates the distance from the 111 Bragg point. We clearly see the extra peak at q=-0.74. The extra peak was observed at 0.78 0.78 0.33 of the Si substrate. In Fig.1(b) the enlargement of (a) around the extra peak is shown. The intensity oscillation is observed, of which period is about 0.22a*. The inverse of this period is roughly equal to the thickness of the oxide layer.

The extra peaks were also observed on the CTR scatterings from the 11-1 and –111 Bragg points. The intensity distributions of the extra peaks along the CTR scatterings have similar oscillation, of which period corresponds to the inverse of the thickness of the oxide layer. These results indicate that the thermal oxide layer on the Si(113) substrate has the quasi-amorphous structure.

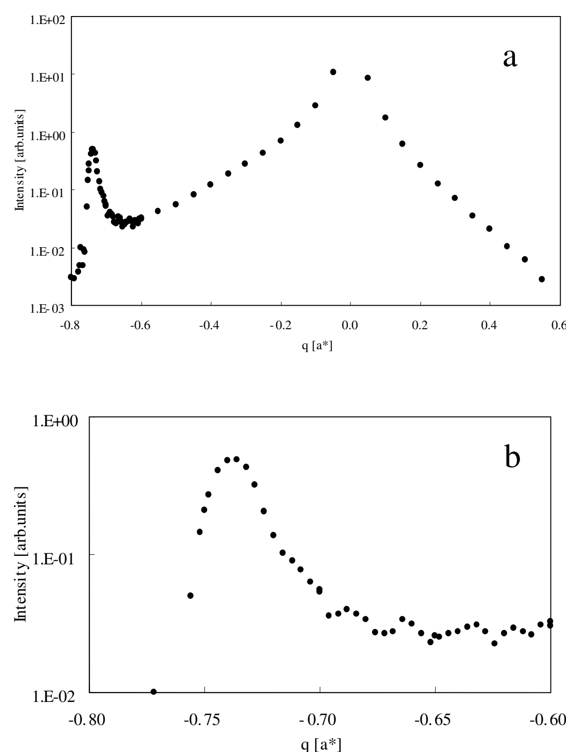

Fig.1 a) Intensity distribution of the CTR scattering from the 111 Bragg point . b) Enlargement of (a) around the extra peak.

References

[1] Y. Iida et al., Surf. Sci. **258**, 235 (1991).
[2] I. Takahashi et al., J. Phys.: Condens. Matter **5**, 6525 (1993).
[3] T. Shimura et al., The Physics and Chemistry of SiO_2 and the Si-SiO_2 Interface 3, (The Electrochemical Society, Pennington, NJ, 1996) p.456.
[4] T. Shimura et al., J. Cryst. Growth **166**, 786 (1996).
[5] T. Shimura et al., Cryst. Res. Technol. **33**, 637 (1998).
[6] H.-J. Mussig et al., Microelectronic Engineering **56**, 195 (2001).

*shimura@mls.eng.osaka-u.ac.jp

10B/2000G111

EXAFS studies on the MCM-41 supported NbC catalysts

Nobuyuki ICHIKUNI*, Hirohisa HACHIYA, Shogo SHIMAZU and Takayoshi UEMATSU
Chiba University, Inage-ku, Chiba 263-8522, Japan

Introduction

Highly ordered inorganic mesoporous material MCM-41, possessing the 2-4 nm pore, has the specific surface area more than 1000 $m^2 \cdot g^{-1}$. Thus, it seemed to be good support for catalyst to maintain the higher dispersion. However, the mesoporous structure was easily destructed by some treatment, especially immersing to solvent and thermal treatment. Moreover, the carburization of bulk Nb_2O_5 into NbC requires relatively high temperature as 1370 K [1]. Although the carburising temperature could be reduced to 1073 K by use of silica support [2], it is still high from calcination temperature. So it seems that it was difficult to prepare NbC/MCM-41 catalyst with highly ordered mesoporous structure.

In this study, we tried to prepare the MCM-41 supported NbC catalysts, and characterized by use of XAFS measurement.

Experimental

Nb_2O_5/SiO_2 precursors were prepared by an impregnation method of SiO_2 (Aerosil #200) or MCM-41 with a $NbCl_5$/methanol solution. The calcined precursor oxide catalyst was carburized in a 20% CH_4/H_2 mixed gas flow to produce NbC/SiO_2 catalyst by TPR process; The samples were heated at a linear rate of 10 $K \cdot min^{-1}$ to 1273 K, which was held until no CO was detected. Catalysts were designated with a kind of silica as NbC/200 or NbC/MCM-41.

Nb K-edge EXAFS spectra were collected at BL-10B of the Photon Factory with Si(311) channel cut monochromator. The sample was transferred into Al cells with Kapton windows. Curve-fitting analyses of EXAFS oscillations in the *k*-space were performed by the EXAFS analysis program REX2000 (Rigaku Co.). Model parameters for curve-fitting analysis (back scattering amplitude and phase shift) were extracted from an EXAFS oscillation observed for bulk NbC (N_1 =12, r_1 =0.315 nm and N_2 = 6, r_2 = 0.446 nm).

Results and discussions

Figure 1 shows the FT of the k^3-weighted EXAFS oscillation. NbC/200 catalyst exhibits the almost same profile as bulk NbC. Although the magnitude of the FT for NbC/MCM-41 is very weak, the profile resembles to the bulk one. The curve-fitting results were summarised in Table 1. Although the FT profiles of the catalysts resembled as bulk NbC, the CN was drastically diminished. As the case of 1st Nb-Nb coordination, CN for NbC/200 and NbC/MCM-41 were 9.5 and 5.4, respectively, suggesting the smaller NbC particles could be constructed on the MCM-41.

From X-ray diffraction analysis and transmission electron microscope observation, the specific hexagonal mesoporous structure of the MCM-41 was maintained for NbC/MCM-41. The design of highly dispersed NbC particle on MCM-41 surface with highly ordered mesoporous structure was achieved by use of the $NbCl_5$ as Nb precursor and the TPR method for carburization.

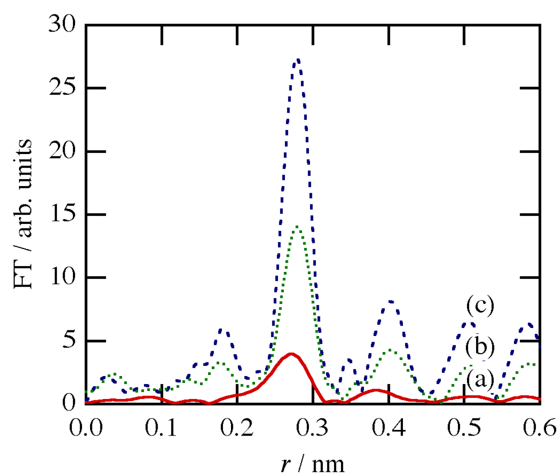

Figure 1. k^3-weighted FT of NbC catalysts; (a) NbC/MCM-41, (b) NbC/200 and (c) bulk NbC.

Table 1: Curve-fitting results for Nb-Nb coordination of supported NbC catalysts

catalyst	N	*r* / nm	d*E* / eV	DW / nm
NbC/MCM-41	5.4	0.311	-6.88	0.0097
	2.0	0.438	-12.6	0.0094
NbC/200	9.5	0.316	2.12	0.0075
	3.1	0.447	1.79	0.0057
bulk NbC (model)	12.0	0.315	0.00	0.006
	6.0	0.446	0.00	0.006

References

[1] V. L. S. Teixeira da Silva, E. I. Ko, M. Schmal and S. T. Oyama, *Chem. Mater.*, **7**, 179 (1995).
[2] N. Ichikuni, F. Sato, S. Shimazu and T. Uematsu, *Topics Catal.*, **18,** 101 (2002).

* ichikuni@tc.chiba-u.ac.jp

11A/2000G171

Magnetic domain imaging of Ni micro-dot array by photoelectron emission microscope (PEEM)

Taichi OKUDA[1*], Takanori WAKITA[1], Ayumi HARASAWA[1], Hideyuki KIWATA[2], Takeshi MATSUSHIMA[1], Takayuki KIHARA[2], Kanta ONO[2], Masaharu OSHIMA[2], Atsushi YOKOO[3], and Toyohiko KINOSHITA[1]

[1]*SRL-ISSP, The University of Tokyo, Kashiwanoha, Kashiwa, Chiba 277-8581, Japan*

[2]*Graduate School of Engineering, The University of Tokyo, Hongo, Bunkyo-ku, Tokyo 113-8656, Japan*

[3]*NTT Basic Research Laboratories, Wakamiya, Atsugi-shi, Kanagawa 243-0198, Japan*

Introduction

The magnetic properties of the small size magnetic elements are recently extensively investigated for the point of view of technological applications, such as high density magnetic storage[1]. It is important to examine the influence of the stray field from neighboring magnetic dots of magnetic dot array when the density of the magnetic dots becomes extremely high. In this paper we report the direct magnetic domain observation of such magnetic dot array of Ni by photoelectron emission microscope(PEEM) with using x-ray magnetic circular dichroism (XMCD) technique in order to examine the interaction between neighboring magnetic dots in the magnetic dot array.

Experimental

Circular, square, hexagonal and triangular shaped Ni micro-dot arrays with the dot size of 10 μm were fabricated on the silicon wafer using electron beam lithography and lift-off techniques. The thickness of the Ni dots were 40 nm. The separation between each dot is 100 nm for the case of the square, hexagonal, and triangular shaped dots.

All the domain imaging of the dot arrays by XMCD-PEEM was performed at room temperature. The circularly polarized soft x-ray light from the off-axis of the bending magnet radiation was injected to the sample at about 18 degree from the sample surface. The magnetic domain images were obtained by dividing the photoelectron images taken at the Ni L_3-edge (hν=877.2 eV) by those of at the L_2-edge (hν=852.7 eV).

Results and discussion

Figure 1(a) shows the magnetic domain images of the portion of the Ni micro-dot array with circular shaped micro-dots of 10 μm. In the figure the circularly polarized soft x-rays were illuminated from downward to upward. Therefore bright and dark regions in the image correspond to magnetic domains positively and negatively magnetized along the direction parallel to the light axis. As shown in the figure many magnetic dots have a magnetic domain contrast with bright and dark part in the right(left) and left(right) half side of the dot. These domain contrasts indicate that the magnetic domain structure is so called flux closure type[1]. Each micro-dot, however, shows an individual domain structure and it seems to have no relation between neighboring dots. In contrast with the circular shaped dot arrays, the magnetic domain structure of the square (Fig. 1.(b)), hexagonal

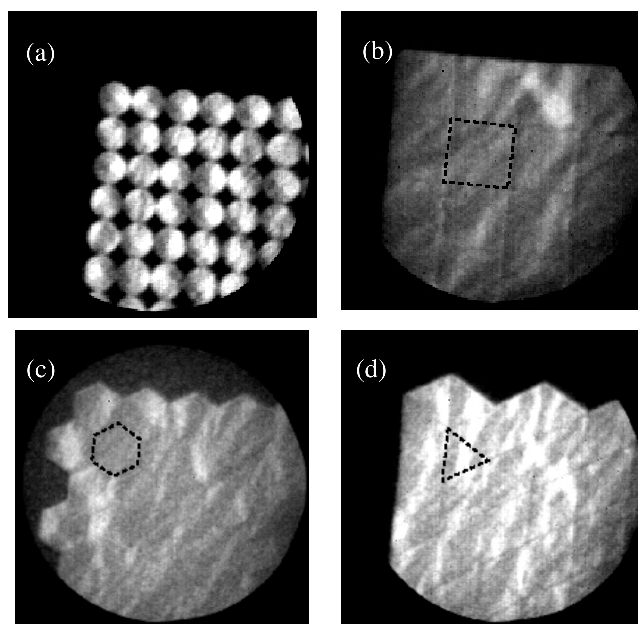

Fig.1 (a) Magnetic domain images of the circular shaped Ni micro-dot arrays with the size of 10 μm. (b) The same as (a) but with the square shaped dots. (c) The same as (a) but with the hexagonal shaped dots. (d) The same as (a) but with the triangular shaped dots. The unit of square, hexagonal and triangular shaped dots are indicated for the eyes.

(Fig. 1(c)), and triangular (Fig. 1(d)) shaped dot arrays seems to have some relation between neighboring dots. That is, the domain structure looks like the magnetic domain structure of continuing Ni sheet and the boundary of the square or hexagonal or triangular dots is not clear. This difference of the magnetic domain structure between circular and other shaped Ni dots may be caused by the difference of the stray field of the dots. Since the circular shaped dot tends to have a flux closure type domain structure, the stray field should be weak and the influence from a neighboring dot is small. In addition, circular shaped dots which are touched by point with neighboring dots, contrast to the other shaped dots which are touched by line, may reduce the influence of the stray field of neighboring magnetic dots.

References

[1] S.P. Li et al., Phys. Rev. Lett. 86, 1102 (2001) and references there in.

*okudat@issp.u-tokyo.ac.jp .

11A/2000G171

Magnetic domain structure of Ni micro-ring observed by photoelectron emission microscope (PEEM)

Taichi OKUDA[1*], Takanori WAKITA[1], Ayumi HARASAWA[1], Hideyuki KIWATA[2], Takeshi MATSUSHIMA[1], Kanta ONO[2], Atsushi YOKOO[3], Masaharu OSHIMA[2] and Toyohiko KINOSHITA[1]

[1]*SRL-ISSP, The University of Tokyo, Kashiwanoha, Kashiwa, Chiba 277-8581, Japan*
[2]*Department of Engineering, The University of Tokyo, Hongo, Bunkyo-ku, Tokyo 113-8656, Japan*
[3]*NTT Basic Research Laboratories, Wakamiya, Atsugi-shi, Kanagawa 243-0198, Japan*

Introduction

The investigation of the magnetic domain structure of small magnetic elements is important for the implementation of the high-density data storage technique. For circular disks the flux closure (FC) domain with central vortex and/or single domain(SD) structures were reported[1][2]. In this paper we report the direct observation of the magnetic domain structure of Ni micro ring by using photoelectron emission microscope (PEEM) combined with x-ray magnetic circular dichroism (XMCD) technique. Such ring–shaped elements have the advantage that a FC structure can be stabilized without the formation of the central vortex, making the FC configuration the energetically more favorable state as compared to the SD state.

Experimental

A series of ring arrays were fabricated on the silicon wafer using electron beam lithography and lift-off techniques. The following rings with outer diameter (d_o) / inner diameter (d_i) were produced (in µm):10/8, 10/6, 10/5, 10/4, 10/2, 10/1, 5/4, 5/3, 5/2.5, 5/2, and 5/1. The thickness of the Ni rings were 40 nm. The rings were arranged in an array of 70×70 m^2 size with a separation equal to $d_o/2$. The XMCD-PEEM experiments were performed at room temperature. The circularly polarized soft x-ray light from the off-axis of the bending magnet radiation was injected to the sample at about 18 degree from the sample surface. The magnetic domain images were obtained by dividing the photoelectron images taken at the Ni L_3-edge (hν=877.2 eV) by those of at the L_2-edge (hν=852.7 eV).

Results and discussion

Figure 1(a) shows the magnetic domain images of the portion of the Ni micro-ring array with d_o/d_i = 10/5,4,2 and 1. The magnetic contrast obtained by the image-dividing method is directly related to the intensity of the magnetic moment on the projection to the light axis. Since the circularly polarized soft x-rays were illuminated from downward to upward, bright and dark regions in the image correspond to magnetic domains positively and negatively magnetized along the light axis. In the rings with d_o/d_i = 10/5, the gradual contrast change from bright region to dark region along the ring periphery is clearly observed. This contrast change corresponds to the FC domain structure as indicated in Fig.1 (b) by arrows showing the direction of the magnetic moment. In the case of the rings with d_o/d_i = 10/4, some rings show the

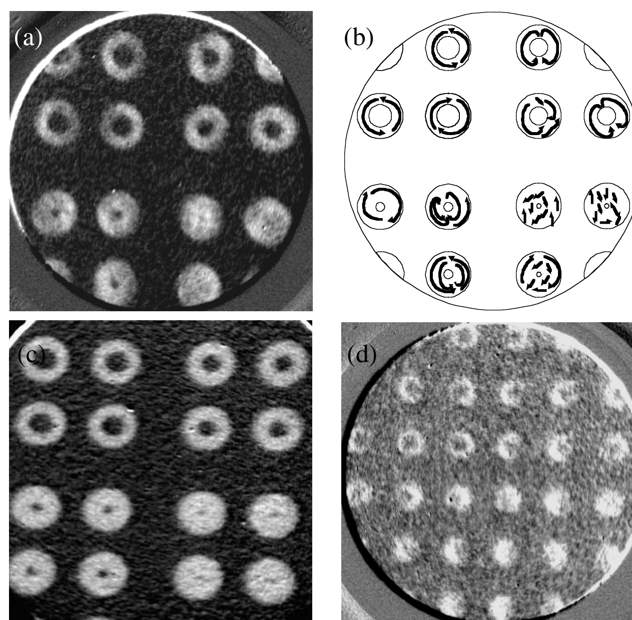

Fig.1 (a) Magnetic domain image of the Ni micro-rings measured by XMCD-PEEM. The outer and inner diameter of the rings are d_o/d_i (in µm) = 10/5, 10/4, 10/2, and 10/1. (b)The magnetic domain structures deduced from (a). Arrows show the direction of the magnetic moment. (c) The same as (a) but after applying magnetic field. (d) The same as (a) but the d_o/d_i =5/2.5, 5/2, 5/1, and 5/0.

onion like domain structure[3] as well as FC structure. The domain structure becomes more complex in the rings with smaller d_i and the rings with d_o/d_i =10/1 show almost multi domain structure. After applying the external magnetic field of about –400 Oe, every domain structure switched to almost perfect SD as shown in Fig. 1(c). Fig. 1(d) is the same as (a) but the d_o/d_i =5/2.5, 5/2, 5/1 and 5/0. As shown in the figure comparing to the larger size ring (d_o= 10 µm), smaller size (d_o= 5µm) ring tends to take a FC structure as recently observed by MFM[1]. Because of the absence of the central vortex in the rings, the exchange energy is reduced substantially and the trend of becoming SD which are observed for the smaller circular disk is suppressed in the ring geometry.

References

[1] S.P. Li et al., Phys. Rev. Lett. **86**, 1102 (2001).
[2] T. Shinjo et al., Science **289**, 930(2000)
[3] J. Rothman et al. Phys. Rev. Lett. **86**, 1098 (2001).

*okudat@issp.u-tokyo.ac.jp

19B/2000G181

Study of Ni/4H-SiC contact by using soft X-ray florescence spectroscopy

Masaaki HIRAI*[1], Akihiko OHI[2], Joselito P. LABIS[2], Chihiro KAMEZAWA[2],
Kenichi YOSHIDA[2], Masahiko KUSAKA[1] and Motohiro IWAMI[1]
[1]Research Laboratory for Surface Science, Faculty of Science,
[2]Graduate School of Natural Science and Technology,
Okayama University, Okayama 700-8530, Japan

Introduction

Silicon carbide (SiC) is one of hopeful materials in hard electronics such as high-power, high-frequency, high-temperature and high-radiation field because of high saturation electron velocity and high breakdown electric field compared with silicon (Si). For the application of electronic devices it is necessary that the physical properties of metal-SiC contact system are clarified.

In this report the partial density of states for Ni/4H-SiC(0001) Si-face contact system is studied by soft X-ray florescence spectroscopy.

Experimental

The samples were prepared as follows.

(i) A wafer of 4H-SiC(0001) Si-face was cleaned by being rinsed in ethyl alcohol, dipped in 5% HF solution and flashed under ultra-high vacuum (UHV) condition.

(ii)Ni metal was evaporated on the surface of this substrate by heating of tungsten boat with Ni wires.

(iii)The sample of Ni/4H-SiC(0001) contact system was thermally treated with electric furnace in flowing H_2+N_2 gases at 600 °C~950 °C for 30 minuets.

The film thickness of evaporated Ni was about 50nm.

The soft X-ray florescence spectroscopy (SXFS) was studied by using a beamline of BL-19B at the SR facility of Photon Factory in KEK. The Si $L_{2,3}$ and C *1s* SXF spectra of the sample, obtained using photon energy of 145eV and 350ev, respectively, were recorded by grating monochromator with a curvature of 5m and position sensitive detector. This SXFS is characterized considering partial density of states in the total energy states due to dipole selection rule of electron transitions.

Results and Discussion

The Si $L_{2,3}$ florescence spectra from Ni/4H-SiC(0001) Si-face contact system is shown in Fig. 1, where the reference spectra from (e) 4H-SiC(0001) Si-face and (d) Ni_2Si are also shown. The spectra of (a) 600 °C, (b) 800 °C and (c) 950 °C are obtained from thermal-treated samples. The spectrum of (e) is characterized by a hump of 86eV, a main peak of 91.3eV, plateau region from 93eV to 96eV and a hump of 97eV. The spectrum of (d) is characterized by a main peak of 90eV and a shoulder from 93eV to 98eV with undulation. The spectra of (a), (b) and (c) has the similar characteristics of the main peak energy and shoulder as (d), but different from the spectrum of (e). Therefore, it is considered that the product of thin film on 4H-SiC mainly contains the Ni_2Si.

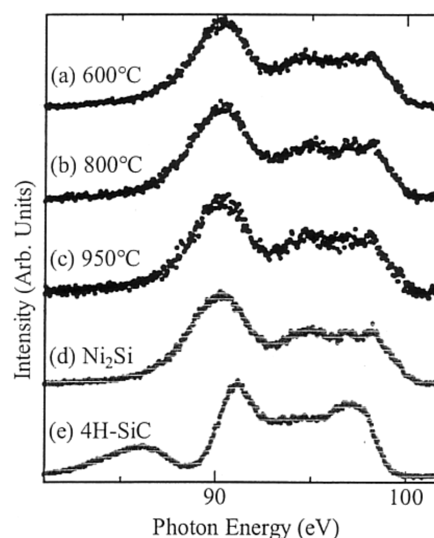

Fig. 1. Si $L_{2,3}$ emission spectra from Ni/4H-SiC(0001) Si-face sample; heated at (a) 600 °C , (b) 800 °C and (c) 950 °C reference ones from (e) 4H-SiC and (d) pressed powder of Ni_2Si [1].

By comparing the spectrum (d) with (a), (b) and (c), it can be concluded that these spectra include the information of the density of states from Ni_2Si. The spectra of C *1s* SXFS are described elsewhere [1].

Summary

These results are summarized as follows.

(1) The interface reacted region is composed of Ni-Si compound silicide and cabide with excess C near the surface region.

(2) The reacted product does not depend on the thermal-treated temperatures.

References

[1] A. Ohi, et al., Applied Surface Science, **190(1-4),** 366-370 (2002).

* hirai@science.okayama-u.ac.jp

15C/2000G200

Strain due to Ni diffusion beneath Hydrogen-terminated Si(111) surface

Takashi EMOTO[1], Koichi AKIMOTO*[1], Ayahiko ICHIMIYA[1], and Kazuyuki HIROSE[2]

[1]Dept. of Quantum Eng., Nagoya University, Furo-cho, Chikusa-ku, Nagoya 464-8603, Japan
[2]Inst. of Space and Astronautical Sci., 3-1-1 Yoshinodai, Sagamihara, Kanagawa 229-8510, Japan

Introduction

Understanding and controlling of silicide reaction are important for improving electronic device technology. Silicide reaction occurs at low temperature between silicon and almost every metal present. These reaction cause problem, such as electric leakage, as the feature size is decreased in large-scale integration (LSI) devices. Hydrogen (H) termination of Si surface is one common technique for controlling the silicide reaction, because hydrogen acts either as a passivating layer or as a surfactant. There have been many studies about metal film growth on hydrogen-terminated Si surfaces. Hirose et al. [1] investigated Ni film growth on a hydrogen-terminated Si(111) surface (Si(111)-H) at room temperature. They found two growth regimes in Ni film growth. Up to deposited Ni film thickness, t_{Ni} = 0.8 nm, Ni atoms migrate into the Si crystal and form an “Ni diffusion layer”. For deposition of the thicker films, Ni films grow on the hydrogen-terminated surface. They suggested that the hydrogen suppresses the silicide reaction at room temperature.

In this paper, we studied affection of this “Ni diffusion layer” to the substrate by using extremely asymmetric X-ray diffraction. Comparing measured and calculated rocking curve, we found that the “Ni diffusion layer” compresses the {111} spacing near Si surface. Moreover such compressive strain fields begin to relax after deposited Ni films become thicker than 0.6 nm[2].

We found that the wavelength dependence of the integrated intensity of the rocking curve is sensitive to the strain fields. From dynamical diffraction calculations, the wavelength dependence is not only sensitive to the strain fields, but is also insensitive to absorption effects of the overlayer [2].

Results and Discussion

The sample were either H-terminated Si(111) or Ni deposited H-terminated Si(111) surfaces. For the Ni deposited Ni films, t_{Ni} = 0.2, 0.4, 0.6, and 0.8 nm. H-terminated surfaces were prepared by dipping of Si wafers in a conventional pH-controlled HF solution.

To evaluate strain fields near sample surfaces, rocking curves of extremely asymmetric Si 113 reflections were measured. The {113} planes of crystals with a diamond structure make 29.5 degrees to the {111} planes. Therefore the rocking curves for the Si 113 reflection strongly reflects distortion of the Si crystal along [111] direction.

Figure 1 shows X-ray wavelength dependencies of the integrated intensities of the measured rocking curves. The integrated intensities can be fitted by using linear functions, as shown in Fig. 1.

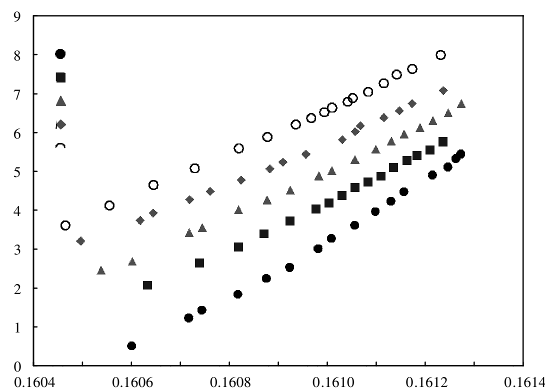

Fig.1 Dependence of integrated intensities for the measured rocking curve.

We quantified the wavelength dependence of the integrated intensities by using the slope, m, of the fitted, linear functions to the X-ray wavelength versus intensity plots. The relation of m to t_{Ni} is shown in Fig. 2.

Fig. 2 Relationship between the slope of the measured integrated intensity vs. X-ray wavelength, and the thickness of deposited Ni.

Figure 2 indicates that with increasing t_{Ni}, for t_{Ni} ’0.6 nm m deceases, but that for t_{Ni} >0.6 nm m increases. We found the slope m is explained by the strain fields near surface[2].

References

[1] K. Hirose, A. Hanta, and M. Uda, Appl. Surf. Sci. **162-163**, 25 (2000) .

[2] T. Emoto, K. Akimoto, A. Ichimiya, and K. Hirose, Appl. Surf. Sci. **190**, 113 (2002).

*akimoto@nucc.cc.nagoya-u.ac.jp

10B/2000G272

In-situ XAFS study of Ag clusters in zeolite 13X

Takafumi MIYANAGA[1]*, Yushi SUZUKI[1], Hideoki HOSHINO[2], Naoyuki MATSUMOTO[1], Takeshi AINAI[2]
[1] Faculty of Science and Technology, Hirosaki University, Hirosaki, Aomori 036-8561, Japan
[2] Faculty of Education, Hirosaki University, Hirosaki, Aomori 036-8560, Japan

Introduction

In the Ag^+-exchanged zeolite the Ag^+ ions are present inside of the zeolite cages, as needed to balance the anionic charge of the zeolite framework. By dehydration under vacuum, silver ions are reduced and then silver clusters are formed in the case of zeolite 4A (Ag-4A) [1,2]. In this report, we study the structural change of Ag clusters in zeolite 13X (Ag-13X) by in-situ XAFS measurements.

Experimental

Ag-13X powder samples were prepared by immersing Na-13X ($Na_{86}[(AlO_2)_{86}(SiO_2)_{106}]246.2H_2O$) zeolite in an aqueous $AgNO_3$ solution at 25℃[2,3]. We prepared two kinds of sample that 86 (Ag_{86}-13X) and 66 Ag^+ ions (Ag_{66}-13X) are replaced by Na^+ ions. The air-dried Ag-13X was set into the in-situ XAFS measurement cell in which the sample can be heated under vacuum. Ag *K*-edge XAFS spectra were measured at BL-10B at 77K in vacuum. A Si(311) channel-cut monochrometer was used, and energy and current of the storage ring were 3.0 GeV and 250~300 mA, respectively. The analyses were performed by XANADU code [4].

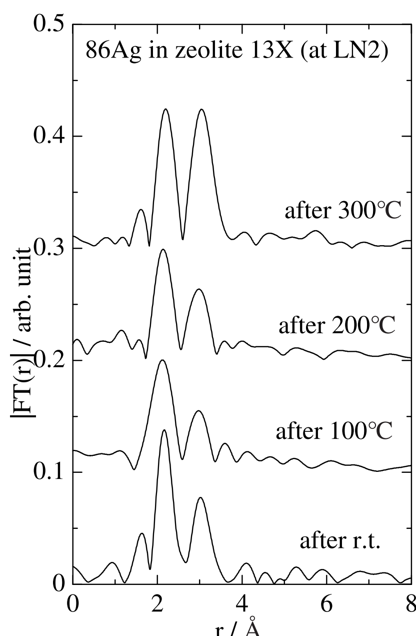

Fig. 1 Fourier transforms of EXAFS for Ag_{86}-13X measured at 77K in vacuum after heated at various temperatures.

Results and Discussion

Figures 1 and 2 show the Fourier transforms (FT) of EXAFS for Ag_{86}-13X and Ag_{66}-13X measured at 77K after heated at various temperatures. It is found that two prominent peaks in the FT: First peak corresponds to Ag-O and second one to mainly Ag-Ag [2]. It is noted that the contribution from Ag-Ag increases at in Ag_{86}-13X 300C and in Ag_{66}-13X at 200C, respectively. For Ag_{12}-13X the prominent increase of the second peak is observed at 100C. It is interesting that the temperature corresponding to the formation of Ag clusters shifts to higher temperature with the increase of the amount of Ag^+ ions in the zeolite cavity. More accurate determination of structural parameters is in progress.

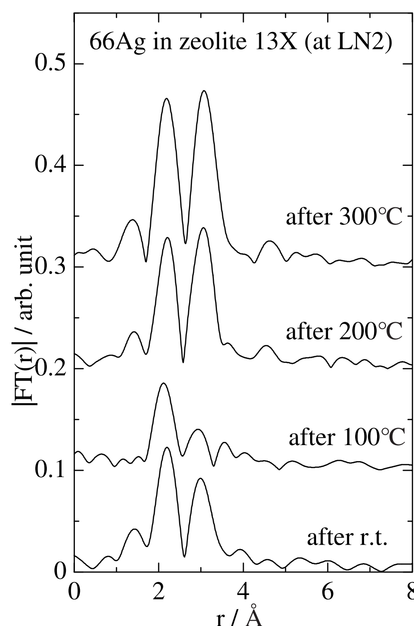

Fig. 2 Fourier transforms EXAFS for Ag_{66}-13X measured at 77K in vacuum after heated at various temperatures.

References

[1]T.Sun and K.Seff, (1994), *Chem. Rev.* **94(4)**, 857-870.
[2]T.Miyanaga, H.Hoshino and H.Endo (2001), *J. Synchrotron Rad.* **8,** 557-559.
[3]H.Hoshino, (1996) *Bulletin of the Faculty of Education, Hirosaki University*, **75**, 29-37 .
[4]H.Sakane, T.Miyanaga, I.Watanabe, N.Matsubayashi, S.Ikeda, S. and Y.Yokoyama, (1993), *Jpn. J. Appl. Phys.*, **32**, 4641-4647.

* takaf@cc.hirosaki-u.ac.jp

9A/2000G276

Polarization dependent total reflection fluorescence XAFS(PTRF-XAFS) studies on Ni atoms dispersed on Al_2O_3(0001) surface

Kaoru IJIMA[1,†], Yuichiro KOIKE[1], Kiyotaka ASAKURA*[1], Yasuhiro TANIZAWA[2], Takafumi SHIDO[2], and Yasuhiro IWASAWA[2]
[1]CRC, Hokkaido University Sapporo 060-0811, Japan
[2]Department of Chemsitry, Graduate School of Science, The University of Tokyo, Hongo Bunkyo-ku, Tokyo 113-0033, Japan

Introduction

Metal deposited on oxides are technologically important. The interaction between metal and oxide is also interesting in a fundamental field. However, it is quite difficult to determine the interface structure between them. EXAFS is one of the promising techniques but the conventional EXAFS provides an average structure over all directions. When the metal is deposited on a single crystal oxide and polarization dependent measurement is carried out, one can get the information about the structure parallel or perpendicular to the oxide surface separately. The method is called as polarization-dependent total reflection fluorescence XAFS(PTRF-XAFS). We have applied this technique to the structure analysis of Ni on Al_2O_3(0001) surface.

Experimental

The details of the the XAFS measurement chamber was described elsewhere[1]. We prepared Ni on Al_2O_3 (0001) using vacuum evaporation. The coverage was estimated by the inflection point of XPS intensities of Ni and O peaks. We measured PTRF-XAFS of Ni/Al_2O_3 sample varying the coverage from 0.02 ML to 2 ML. The XAFS measurement was carried out at BL9A using a Si(111) double crystal monochromator. We accumulated the fluorescence data using a 19-element SSD.

Results and discussion

Fig.1 shows the XAFS oscillations with two directions, parallel to the surface (s-pol) and perpendicular to the surface (p-pol) for 0.04 ML Ni/Al_2O_3 (0001). The XAFS oscillation changed at about 0.1 ML where Ni-Ni started to be observed, indicating the Ni agglomerated to particles at more than 0.1 ML. Here we report the details in the analysis of Ni local structure less than 0.1 ML where Ni was present in an atomically dispersed form.

We carried out FEFF calculations based on a several model structures. As a result, the EXAFS oscillation is found to be due to the scattering from the oxygen and the polarization dependence of coordination number indicated the Ni is located on the three fold site. There is 3 types of three fold sites on the surface of Al_2O_3 (0001) called as A,B and C sites as shown in Fig. 2. Site A is the one theoretically predicted[2]. However, Al should be present below the Ni with Ni-Al distance at about 0.191 nm in the site A. In our EXAFS could not be reproduced when such a short Ni-Al distance was present. Site C is usually occupied by the surface Al. If Ni is adsorbed on this site C, Al is replaced with the Ni. Site B is the one where the next Al should be placed.

We can reproduce the EXAFS oscillation by assuming the Ni location at the Site B but not at the site C. Site C does not have no surface Al contribution to the EXAFS oscillation and hence s pol could not be well simulated.

In summary, the Ni is placed on the B site of Al_2O_3(0001) where the next Al is expected to sit and the conclusion is contradicted with the previous calculation.

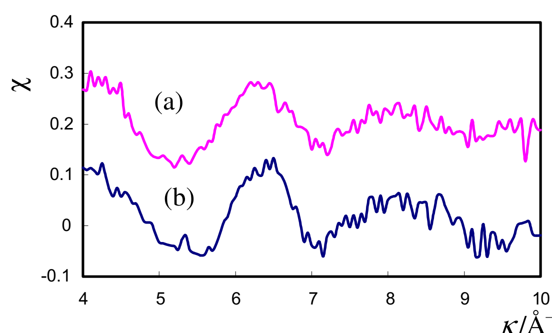

Fig.1 XAFS oscillation of Ni/Al_2O_3 (a): spol, (b): ppol

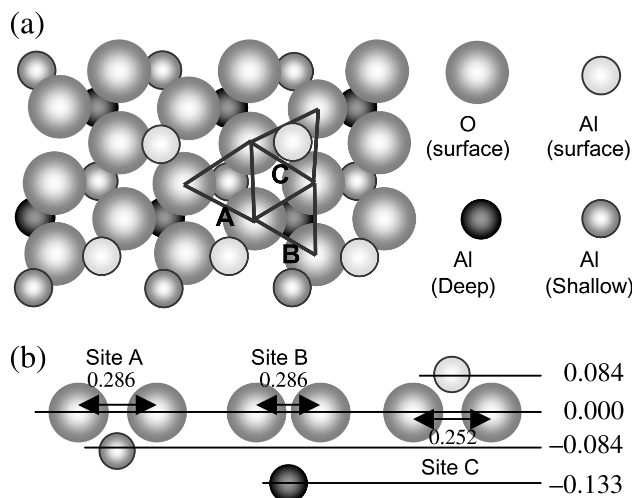

Fig.2 Al_2O_3 (0001) surface structure. (a) top view, (b) side view.

References

[1] W. J. Chun, et.al. J.Synchrotron Rad., **8**, 168 (2001).
[2] Q. Ma,et.al. J.Phys.Chem., **105**, 2212 (2001).

†present address: Department of Electrical Engineering, Yamanashi University, Takeda 4-3-11, Kofu 400-8511, Japan

13C/2000G280

Formation process of β-$FeSi_2$ on Si (111) substrate studied by means of SR-XPS

Takeru SAITO[1], Hiroyuki YAMAMOTO[1], Masaharu HARAGUCHI[2], Motoyasu IMAMURA[3], Nobuyuki MATSUBAYASHI[3], Tomoaki, TANAKA[3], Hiromichi SHIMADA[3], Kiichi HOJOU[1],
[1]Japan Atomic Energy Research Institute, 2-4 Shirakatashirane, Tokai, Naka, Ibaraki 319-1195, Japan
[2]Graduate school of Science and Engineering, Ibaraki University, 2-1-1, Bunkyo, Mito, Ibaraki 310-8512, Japan
[3]National Institute of Advanced Industrial Science and Technology, 1-1 Higashi, Tsukuba, Ibaraki 305-8565, Japan

Introduction

Recently, semiconducting iron silicide, β-$FeSi_2$ has attracted lots of attention because of its direct band gap of 0.85 eV [1]. From this reason, formation processes of β-$FeSi_2$ on Si substrates have widely been investigated. However, the reaction mechanisms between Fe and Si are not yet clearly understood.

In the present study, we study the formation mechanisms of β-$FeSi_2$ on Si (111) surface during solid-phase epitaxy (SPE) process by means of XPS using synchrotron radiation (SR-XPS).

Experimental

All the experiments were done at the beam-line 13C of the Photon Factory. The XPS spectra were recorded with a hemispherical electron analyzer (PHI 1600C).

The substrate used was a Si wafer oriented with [111] direction. Fe was deposited with a thickness of 1.0 nm at room temperature. After the Fe deposition, the substrate was stepwise annealed for 15 min at 523 K, 723 K, and 973 K.

Results and discussion

Figure 1 shows changes in the Fe/Si atomic ratios with the annealing temperature as a function of excitation energies. The atomic ratios were calculated from the peak intensities and photo-ionization cross-sections of Fe 3p and Si 2p spectra. After Fe deposition at room temperature (a), the Fe/Si ratio is rapidly increased with decreasing the excitation energy. This indicates the formation of a thin Fe layer on Si (111). With rising annealing temperature, the Fe/Si ratios become small indicating the compositional changes by the annealing.

To investigate the Fe/Si depth distribution in detail, two sets of simulation were performed. In the model 1, a Fe over-layer with a thickness of t homogeneously covers the Si surface. In the model 2, an over-layer with a thickness of t and a Fe/(Fe+Si) atomic ratio of a_0 homogeneously covers another layer with a Fe/(Fe+Si) atomic ratio of a_1. The Fe/Si atomic ratio at each excitation energy (hν) can be given by the following equations:

$$\left[\frac{Fe}{Si}\right]_{h\nu} = \frac{\int_0^\infty \exp(-z/\lambda_{Fe}\sin\theta)dz}{\int_0^\infty \exp(-z/\lambda_{Fe}\sin\theta)\exp(-(z-t)/\lambda_{Si}\sin\theta)dz} \quad \text{(Model 1)}$$

$$\left[\frac{Fe}{Si}\right]_{h\nu} = \frac{\int_0^t a_o \exp(-z/\lambda_{Fe}\sin\theta)dz + \int_t^\infty a_1 \exp(-z/\lambda_{Fe}\sin\theta)dz}{\int_0^t (1-a_o)\exp(-z/\lambda_{Si}\sin\theta)dz + \int_t^\infty (1-a_1)\exp(-z/\lambda_{Si}\sin\theta)dz} \quad \text{(Model 2)}$$

The details of simulation are described elsewhere [2].

The experimentally obtained profile for the smple before annealing is well fitted by a simulated profile using the Model 1 with t = *1.07 nm*. On the other hand, the profile of the sample after annealing at 523 K was fitted by simulation using Model 2 and $a_0 = 0.9$, $a_1 = 0.1$ and t = *0.34 nm*. This result indicates that the substrate surface is covered by a thin Fe-rich layer and that Si diffused into the Fe layer.

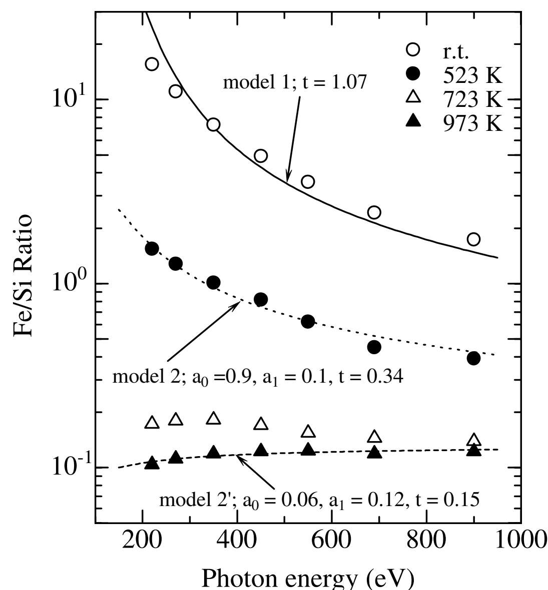

Fig. 1 Changes in the Fe, Si atomic ratios during SPE process recorded with different excitation energies

After annealing at 723 K, the Fe/Si atomic ratios become almost independent of the excitation energies. This indicates the chemical composition is even from the surface to the largest analysis depth. The results of Fe 2p and valence-band spectra suggest the formation of β-$FeSi_2$. However, the obtained Fe/Si atomic ratio, *0.2* is relatively small compared with the stoichiometric atomic ratio of β-$FeSi_2$ *(0.33)*. This may be attributed to the aggregation of β-$FeSi_2$ on the surface.

After annealing at 973 K, the simulated profile using a parameter set of $a_0 = 0.06$, $a_1 = 0.12$ and t = *0.15 nm* can be compared with the experimental data. This result clearly suggest the formation of thin Si layer at topmost of the surface.

References

[1] N. E. Christensen, Phys. Rev. B, **42**, 7148 (1990)
[2] T. Saito et al., Anal. Sci., **17** Supplement, i1073 (2001)

* tsaito@popsvr.tokai.jaeri.go.jp

9A, 10B/2000G283

In-situ XAFS observation of USY supported Pd-Pt catalysts during sulfidation process

Kyoko K. BANDO*, Takashi MATSUI, Lionel LE BIHAN, Koichi SATO, Tomoaki TANAKA,
Motoyasu IMAMURA, Nobuyuki MATSUBAYASHI, Yuji YOSHIMURA
National Institute of Advanced Industrial Science and Technology, Tsukuba, Ibaraki305-8565, Japan

Introduction

Ultra stable Y-type zeolite supported Pd-Pt catalysts show higher activity for hydrogenation of aromatic compounds in the presence of sulfur, compared with monometallic supported Pd or Pt catalysts. However, either the real structure of active metal species under the reaction conditions, or the reason for promotion in sulfur tolerance as observed in hydrotreating conditions is not yet clear for the bimetallic Pd-Pt species. In order to clarify this point, we carried out an *in-situ* X-ray absorption fine structure (XAFS) spectroscopy analysis of the Pd-Pt catalysts and elucidated structural change of surface species during reduction and sulfidaiton process.

Experimental

Supported Pd-Pt (molar ratio of Pd/Pt was 4) bimetallic catalysts (Pd-Pt/USY for short) were prepared using ultra stable Y-type zeolite (USY, SiO_2/ Al_2O_3 = 13.9) by impregnation method. The precursors were $Pd(NH_3)_4Cl_2 \cdot xH_2O$ (41.21 wt% Pd) and $Pt(NH_3)_4Cl_2$ xH_2O (55.6 wt% Pt). The total metal content was 1.2 wt%. The impregnated samples were dried in vacuum at 333 K for 6 h, then calcined at 573 K under oxygen flow for 3 h. Pd K-edge and Pt L_{III}-edge XAFS measurements were made in a transmission mode at BL10B and 9A. The sample was pressed into a round disc and set in an *in-situ* cell designed for measurements under a flow of a reactant gas. Figure 1 shows a schematic diagram of XAFS observation system designed for measurement under sulfidation conditions. Exhausted H_2S was absorbed in a 20 % NaOH aqueous solution and H_2 was burned and converted into water by a burner set at the end of the system. After all the toxic and flammable gases were removed, the effluent gas was led to a duct. XAFS spectra were observed by step scanning mode with a data accumulation time of 0.5 – 1 sec for each step. XAFS analysis of the obtained data was conducted with commercially available software (REX, Rigaku Co.).

Results and discussion

After reduction at 573 K, the catalysts were sulfided at 553 K under a flow of H_2S (100ppm) /H_2 (20%) /Ar (balance). Figure 2 shows Fourier transform of Pt L_{III}-edge EXAFS spectra observed for Pd-Pt/USY during sulfidaiton. The peak at 0.20 nm is assigned to Pt-S scattering and it already appeared at 20 min and became dominant at 100 min. Sulfidation of Pt proceeded much faster than that of Pd, where the Pd-S peak became dominant at 140 min. This fact suggests that Pt species located on a sulfur-accessible position. Possible structures expected for reduced Pd-Pt active metal species on the surface are: (1) fine Pt metal particles were located on the surface of large Pd metal particles, or (2) primary monometallic (Pd or Pt) particles gathered randomly and formed larger bimetallic metal particles. To clarify this point, precise analysis of EXAFS spectra is now in progress.

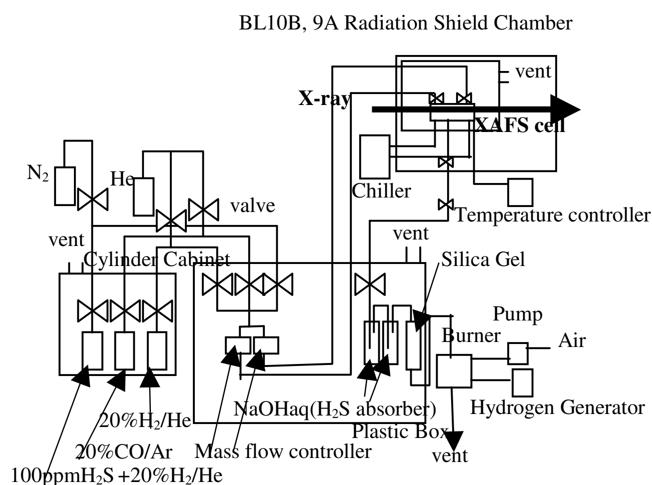

Fig.1 Schematic diagram of an in-situ XAFS system designed for measurements under reaction conditions.

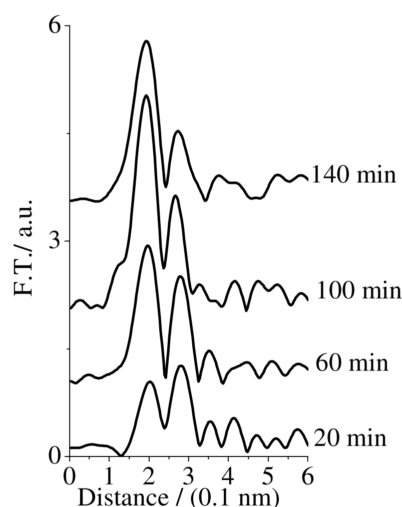

Fig.2 Change in Fourier transform of Pt L_{III}-edge EXAFS spectra with elapsed time observed during sulfidation in a flow of H_2S(100 ppm)/H_2(20%)/Ar for Pd-Pt/USY.

* kk.bando@aist.go.jp

10B/2000G286

In-situ XAFS characterization of Mo/SiO_2 catalyst during propene photometathesis reaction

Haruno MURAYAMA[1], Nobuyuki ICHIKUNI*[1], Kyoko K. Bando[2], Shogo SHIMAZU[1] and Takayoshi UEMATSU[1]
[1]Chiba University, Inage-ku, Chiba 263-8522, Japan
[2]National Institute of Advanced Industrial Science and Technology, Tsukuba 305-8585, Japan

Introduction

Photocatalytic activities of supported molybdenum oxide catalysts are strongly affected by their local structures. Characterization of active sites under reaction state is important to understand the photocatalysis. Since, the structure under reaction condition was often differed from under static state [1].

The Mo/SiO_2 catalysts, prepared by photochemical anchoring (PCA) method, are expected to have the designable Mo surroundings. In other words, the distance between dimeric Mo atoms can be finely designed by control of the irradiation energy. In this study, the changes of local structure on PCA Mo/SiO_2 catalysts under propene photometathesis reaction and the effect of local structure to photocatalysis were investigated by *in-situ* XAFS technique.

Experimental

5wt% Mo/SiO_2 catalysts were prepared by dry-mixing of the $Mo_2(CH_3CO_2)_4$ and the pre-evacuated silica (CARiACT P-10) under UV irradiation through UV35 filter (λ>350 nm) or without filter (λ>250 nm) at room temperature for 1 h *in vacuo*. The catalysts were treated with H_2, followed by O_2 at 473 K. The catalyst was designated with UV cut-off filter's wavelength as PCA35 or PCA25.

Mo K-edge EXAFS measurements were carried out at BL-10B (PF) with a Si(311) channel cut monochrometer. *In-situ* EXAFS spectra under propene photometathesis reaction were collected using specially designed SUS cell as depicted in Fig. 1. The cell has a quartz glass window in order to penetrate the UV light to the sample disks. The catalysts were pressed into self-supporting disks and settled in the cell. The reaction was carried out at room temperature with 40 $cm^3 \cdot min^{-1}$ flow of propene under irradiation by using a 75 W high-pressure Hg lamp.

Results and discussion

Figure 2 shows the EXAFS Fourier transforms for the pretreated catalysts and those under the reaction condition. The curve-fitting analyses in the *k*-space were performed by using K_2MoO_4 and MoO_3 as references. On PCA25, there are no differences between *ex-situ* and *in-situ* condition. It suggests that Mo=(:CH_2) bond (intermediate) resembled to Mo=O bond (initial state) on PCA25, and hence EXAFS could not distinguish the differences between *ex-situ* and *in-situ* conditions.

The Mo-(O)-Mo bond distances of PCA35 and PCA25 were 0.31 and 0.33 nm, respectively. CN and bond distance of Mo-O and Mo-(O)-Mo on PCA35 decreased under the reaction condition, indicated that Mo=(:CH_2) led to the unequalness of active sites. Since the Mo-(O)-Mo bond distance of PCA35 was short, an activated Mo=O site might be stabilized by the connected neighbouring Mo=O bond. On the other hand, Mo=O site of PCA25 acted independently from the neighbouring Mo. The structural changes of Mo/SiO_2 depending on Mo-(O)-Mo bond distance were observed by this technique.

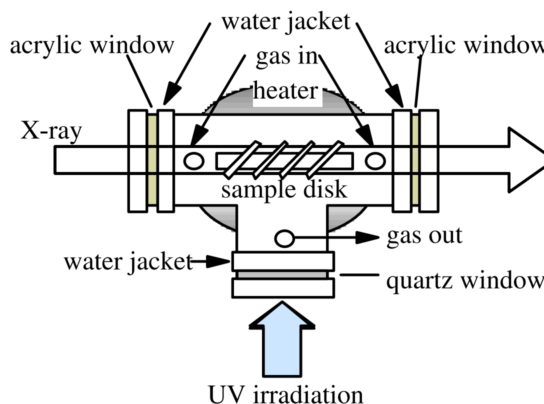

Fig. 1. Schematic of *in-situ* XAFS cell.

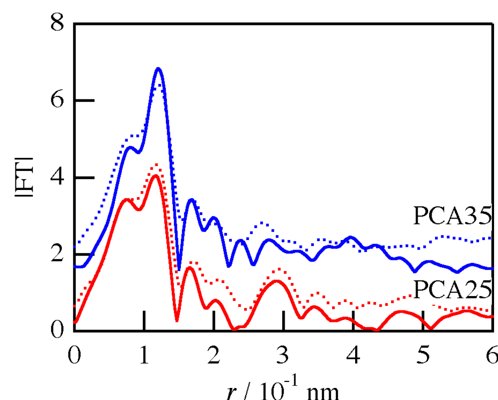

Fig. 2. FT spectra for Mo/SiO_2 catalysts; (solid line) pretreated, (dotted line) under propene photometathesis reaction.

Reference

[1] N. Ichikuni, H. Murayama, K. K. Bando, S. Shimazu and T. Uematsu, *Anal. Sci.*, **17s**, i1193 (2001).

* ichikuni@tc.chiba-u.ac.jp

Crystal orientation of silver films on silicon surfaces

Atsushi HATA[1], Koichi AKIMOTO*[1], Shinji HORII[1], Takashi EMOTO[1], Ayahiko ICHIMIYA[1], Hiroo TAJIRI[2], Toshio TAKAHASHI[2], Hiroshi SUGIYAMA[3], Xiaowei ZHANG[3], and Hiroshi KAWATA[3]

[1]Dept. of Quantum Eng., Nagoya University, Furo-cho, Chikusa-ku, Nagoya 464-8603, Japan
[2]Institute for Solid State Physics, University of Tokyo, 5-1-5 Kashiwanoha, Kashiwa 277-8581, Japan
[3]Photon Factory, High Energy Accelerator Research Organization, Tsukuba 305-0801, Japan

Introduction

The effects of reconstructed structures on the preferred orientation of overlayer films have not been fully understood, while the control of the crystal orientation of overgrown films is needed in all electric devices.

The Ag-induced ($\sqrt{3}\times\sqrt{3}$)R30 structure on a Si(111) surface (called Si(111)$\sqrt{3}$-Ag for short) has been much interested by many researchers. The surface Si(111)$\sqrt{3}$-Ag structure has been explained by a honeycomb-chained-triangle (HCT) model[1,2]. Recently, the $\sqrt{3}$ structure has been reported to exist at the Ag/Si(111)$\sqrt{3}$-Ag interface[3,4]. As for Ag overlayer films on the $\sqrt{3}$ structure, some articles [3,5] has been reported on the growth mechanism and/or initial-stage structural model. However, the relation between reconstructed structures and the preferred orientation of overlayer films has not been fully understood.

Results and Discussion

The Si(111)$\sqrt{3}$-Ag surface was obtained by depositing 1ML Ag on the Si(111)7×7 surface at about 790K. After preparation of the Si(111) $\sqrt{3}$-Ag, 50ML Ag was deposited on the Si(111) $\sqrt{3}$-Ag at the substrate temperature of 50~300K. The RHEED pattern taken after the deposition of 50ML-thick Ag overlayers showed no $\sqrt{3}$ pattern. However, the Ag(50ML)/Si(111) $\sqrt{3}$-Ag showed intense $\sqrt{3}$ fractional order reflection peaks by grazing incidence X-ray diffraction measurements. This is the evidence to show that the $\sqrt{3}$ structure remains at the interface[3,4].

In order to study the crystal orientation of Ag thin films on a Si(111)$\sqrt{3}$-Ag surface, scans of X-ray measurements were made by rotating the sample about the surface normal (θ- scan). The Ag{111} plane was mainly grown on the surface[3]. In addition, the Ag 111 reflection was measured. The scan results for the sample with 50ML-Ag deposition on a $\sqrt{3}$ surface at 300K and 50K were shown in Fig. 1. In Fig. 1, a peak at θ=0° was separated in two. The separation angle was about 8°. This separation was already reported[3], but a clear explanation has not been given. In order to clarify the origin of this separation, we measured mesh scan for the sample with 50ML-Ag deposition on a $\sqrt{3}$ surface at 300K. We found streaky scattering along the [11$\bar{2}$] direction parallel to the surface as shown in Fig. 2.

The streaky scattering is thought to originate from the CTR (crystal truncation rod) scattering from a sidewall plane of the Ag {111} nanometer-scale crystals as shown in Fig. 4. The sidewall plane of the Ag {111} should be the {11$\bar{2}$} plane, because the streaky scattering was appeared along the [11$\bar{2}$] direction.

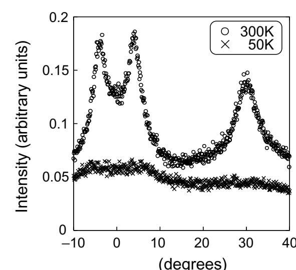

Fig.1 Intensity profiles of Ag bulk reflections for Ag/Si(111)$\sqrt{3}$-Ag for the Ag 111 reflection.

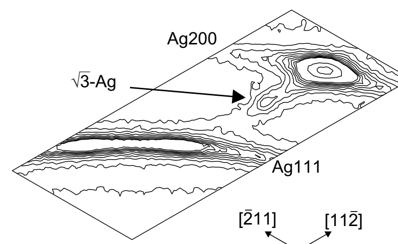

Fig. 2 Measured mesh scan for Ag/Si(111)$\sqrt{3}$-Ag.

References

[1] T. Takahashi, S. Nakatani, N. Okamoto, T. Ishikawa, S. Kikuta, Jpn. J. Appl. Phys. **27**, L753 (1988).
[2] T. Takahashi and S. Nakatani, Surf. Sci. **282**, 17 (1993).
[3] K. Akimoto, M. Lijadi, S. Ito, and A. Ichimiya, Surf. Rev. Lett. **5**, 719 (1998).
[4] S.Horii, K.Akimoto, S.Ito, T.Emoto, A.Ichimiya, H,Tajiri, W.Yashiro, S.Nakatani, T.Takahashi, H.Sugiyama, X.Zhang, and H.Kawata, Surf. Sci. **493**, 194 (2001).
[5] R.D.Aburano, H.Hong, J.M.Roesler, K.Chung, D.-S.Lin, P.Zschack, H.Chen, and T.-C.Chiang, Phys. Rev. **B52**, 1839 (1995).

*akimoto@nucc.cc.nagoya-u.ac.jp

15B2/2000S2-003

Temperature dependence of the Si(111)-$\sqrt{3}\times\sqrt{3}$-Ag structure

Hiroo TAJIRI[1], Kazushi SUMITANI[1], Toshio TAKAHASHI*[1]
Koichi AKIMOTO[2], Hiroshi SUGIYAMA[3], Xiaowei ZHANG[3], Hiroshi KAWATA[3]
[1]ISSP, The Univ. of Tokyo, Kashiwanoha, Kashiwa, Chiba 277-8581, Japan
[2] Dept. Quantum Eng., Nagoya Univ., Furo-cho, Chikusa-ku, Nagoya 464-8609, Japan
[3]KEK-PF, Tsukuba, Ibaraki 305-0801, Japan

Introduction

The structure of Si(111)- $\sqrt{3}\times\sqrt{3}$-Ag had been in controversy for years until a honeycomb chained triangle (HCT) model was proposed[1]. Since then, the HCT model has been supported by various kinds of surface science techniques. Recently, however, a new model called inequivalent triangle (IET) model has been proposed by first-principles calculations[2] and STM studies at low temperatures[3]. Thus the IET model casts doubts on the HCT model. For this reason, we study temperature dependence of the Si(111)-$\sqrt{3}\times\sqrt{3}$-Ag structures, and discuss the phase transition of the surface in this report.

Figure 1(a) and 1(b) show the HCT and IET models. The IET model is characterized as a structure in which a large Ag triangle indicated dashed lines in the HCT model is rotated around its center by about 6 degrees. As a result, the IET model, losing a mirror line, has a lower symmetry in comparison with the HCT model.

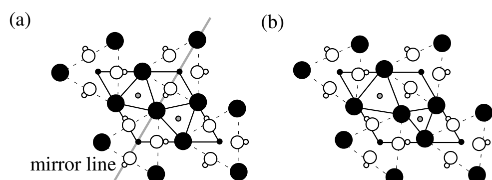

Fig.1. A honeycomb chained triangle (HCT) model(a) and an inequivalent triangle (ITE) model(b).

Experimental results and discussions

Experiments using grazing incidence X-ray diffraction were performed at BL-15B2. Figure 2(a) and 2(b) show Patterson maps calculated from intensity distributions obtained at RT and LT(50K). A single peak indicated A in Fig.2(a) splits into two peaks, A1 and A2, in Fig.2(b). This means that Ag atoms take the HCT structure at RT and they change into the IET structures at LT. Two peaks correspond to two domains in a relation of surface twins in which Ag triangles are rotated in opposite directions. Detailed analysis of the least squares fit also showed the same results for both data where anisotropic Debye-Waller factors were used. Ag atoms making triangles are found to be vibrating mainly in the rotational directions, particularly at RT.

Next we observed temperature dependence of some diffraction spots from RT to 50K. At low temperatures diffuse scattering due to surface twins is observed. From temperature dependence of the integrated intensities of diffuse scattering, it was found that the phase transition temperature is about 150K , and the critical exponent beta takes a large value of 0.27. We also analyzed temperature dependence of the integrated intensities of Bragg components. Their intensities changed at the phase transition temperature.

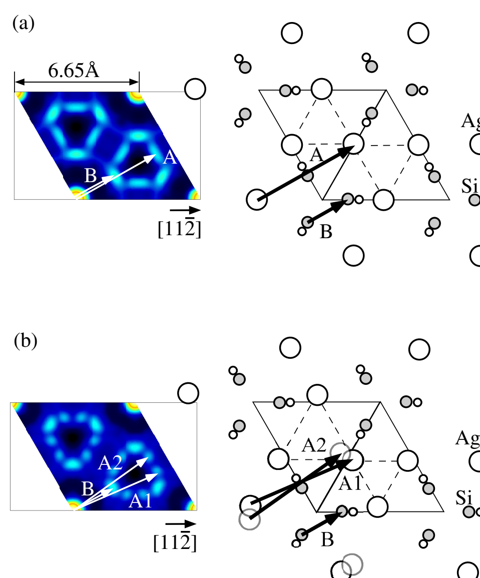

Fig.2. Patterson maps calculated from the integrated Bragg intensities of diffraction spots observed at room temperature (a) and a low temperature of 50K(b).

In summary, the structure of Si(111)-$\sqrt{3}\times\sqrt{3}$-Ag was determined to be the HCT structure with strong anisotropic thermal vibrations at RT and the IET structure with surface twins at LT. The phase temperature and critical exponent of the surface were determined. Order-disorder phase transitions are not favored; honeycomb protrusions observed in STM images at RT are not interpreted as thermal fluctuations between twin states. The present work rather supports a displacive type phase transition.

References

[1] T. Takahashi et al., Jpn. J. Appl. Phys. **27**, L753 (1988), Surf. Sci. **282**, 17 (1993).
[2] H. Aizawa et al., Surf. Sci. Lett. **429**, L509 (1999).
[3] N. Sato et al., Surf. Sci. **442**, 65 (1999).
* ttaka@issp.u-tokyo.ac.jp

1C/2001C009

Chemical structure of the SiO_2/Si(001) interface formed at high temperatures

Hiroo OMI, Satoru SUZUKI, Yoshio WATANABE, and Toshio OGINO
NTT Basic Research Laboratories, Atsugi, Kanagawa, 243-0198 Japan

An understanding of thermal silicon oxidation is essential for further advancements in semiconductor science and technology. Of particular importance is that we clarify the mechanism of the morphological evolution between the growing thermal silicon oxide layers and Si(001) substrate during oxidation so that we can obtain an abrupt interface on an atomic scale. This is because the morphological features, including roughness and atomic steps at the SiO_2/Si(001) interface seriously degrade the dielectronic properties of silicon devices, such as metal-oxide-semiconductor filed emission transistors (MOSFETs).

Thermal silicon oxidation, in general, can be categorized according to oxidation temperature as low-temperature (400 – 1100°C) or high-temperature [1100 – 1414°C (melting point of Si)] oxidation. Thermal oxidation at low temperature is widely used to obtained insulating silicon oxide layers in conventional Si devices, and the chemical structure of the SiO_2/Si(001) interface has been extensively studied so far. Thermal silicon oxidation at high temperature, on the other hand, is becoming important for advanced silicon devices based on silicon-on-insulator (SOI) structures.[1] However, little attention has been paid to the chemical structure of the high-temperature thermally grown silicon oxide layers on Si(001) and its interface.[2] The chemical information at the interface is essential for understanding the origin of the interface roughness.

Here, we report a photoemission study of the thermally grown SiO_2 on Si(001) at high-temperature.

We used B-doped Si(001) wafers with miscut angle of 1°. The wafers were thermally oxidized in conventional electronic furnace. The wafers were subjected to various annealing conditions in an Ar atmosphere containing a small constant fraction of O_2 gas (0.2%). Annealing temperatures and times were 1200, 1250, and 1325°C, and 2.5, 4, and 2.5 h. The silicon oxide layers were etched back in dilute HF solution (1%) followed by DI water rinse. The etchback oxide thickness was less than 5 nm and the etchback treatment did not destroy the buried SiO_2/Si interface.

A typical spectrum recorded at 240 eV photon energy from a 1250°C sample shows that different suboxide peaks are clearly observed in the raw data. The peaks can be assigned to the suboxide states (Si^{+1}, Si^{+2}, Si^{+3}, Si^{+4}). The intensities of the Si^{+1}, Si^{+2}, Si^{+3} peaks become strong with increasing incident beam energies, indicating that the suboxide states are localized at the interface. The observed intensity distribution is quite different with that of the SiO_2/Si(001) interface formed at low temperatures. This discrepancy means that the high-temperature thermal silicon oxidation produces the original chemical states at the interface.

References

[1] H. Omi, D. J. Bottomley, and T. Ogino, Appl. Phys. Lett. **80,** 1073 (2002).

[2] D. Bottomley, H. Omi, Y. Kobayashi, M. Uematsu, H. Kageshima, T. Ogino, Phys. Rev. **B66,** 035301 (2002).

*homi@will.brl.ntt.co.jp

9A/2001C014

P and S K-edge XANES measurements of tribofilms formed on steel disks in conversion electron yield and fluorescence yield modes

Yoshimu IWANAMI*[1], Toru MAKISHIMA[1], Takaki OKUBO[1], and Masaharu NOMURA[2]
[1]Nippon Mitsubishi Oil Corp oration, 8, Chidoricho, Naka-ku, Yokohama, 231-0815, Japan
[2] Institute of Materials Structure Science, KEK-PF, 1-1 Oho, Tsukuba, Ibaraki 305-0801, Japan

Introduction

The fuel efficiency of vehicles will continue to be an important issue, due to the needs to conserve natural resources and protect the global environment. One of the ways to improve fuel efficiency is to control the lubricating properties of oils used in the lubricated parts of vehicles. Additive formulations in oils are important to control the lubricating properties. For example, formulations to reduce the friction coefficients of engine oils and to enhance the friction coefficients of transmission oils are needed. Therefore, we have studied tribofilm chemistry in order to understand the effects of additive formulations on the lubricating properties of both engine and transmission oils.

In this report, we summarize the results of P and S K-edge XANES measurements of tribofilms formed on steel disks.

Experimental

Tribofilms were formed on steel disks with the oils formulated for different friction coefficients as described Table 1, using a friction testing machine. The disks were cleaned with n-hexane prior to the XANES measurements.

P and S K-edge XANES measurements were carried out in conversion electron yield (CEY) and fluorescence yield (FY) modes, using a Lytle detector at BL-9A.

Table 1: XANES-measured tribofilms

Tribofilm	Oil	Friction coefficient	XANES mode[1)]	
			CEY	FY
E-H-μ	Engine oil	High	×	○
E-M-μ	Engine oil	Middle	×	○
E-L-μ	Engine oil	Low	○	○
T-H-μ	Transmission oil	High	○	○
T-L-μ	Transmission oil	Low	○	○

1) ○: measured, ×: unmeasured

Results and Discussion

Tribofilms formed by engine oils

Figure 1 shows the S K-edge XANES spectra of tribofilms formed by three different engine oils measured in the FY mode (bulk analysis). It is obvious from the figure that the spectra are significantly different. This suggests that the sulfur composition in the bulk of tribofilms may be different depending on the additive formulation of the engine oils.

In contrast, all the P K-edge XANES spectra (not shown) of the tribofilms measured in the FY mode are almost identical, suggesting that the phosphorous composition in the bulk of tribofilms may be similar.

Tribofilms formed by transmission oils

Figure 2 shows the S K-edge XANES spectra of tribofilms formed by two different transmission oils, measured in both the FY (bulk analysis) and CEY mode (surface analysis). In the figure, the spectra are different, suggesting that the sulfur composition in the tribofilms may be different, depending on the additive formulation of the transmission oils. Furthermore, the spectra of both the T-H-μ and T-L-μ tribofilms measured in the FY and CEY modes are different. This suggests that the sulfur compositions in the bulk and surface of the tribofilms may be different, and that surface modifications may take place in the tribofilms.

In contrast, all the P K-edge XANES spectra (not shown) of the tribofilms measured in both the FY and CEY modes are almost identical, suggesting that the phosphorous composition in the bulk and surface of tribofilms may be similar.

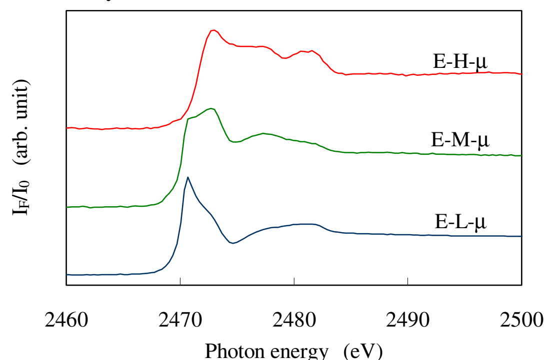

Figure 1 S K-edge XANES spectra in the FY mode of tribofilms formed by engine oils.

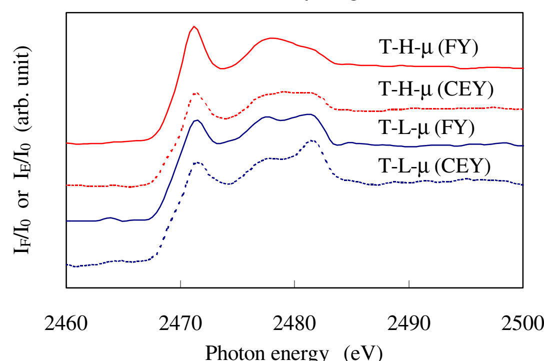

Figure 2 S K-edge XANES spectra in the CEY and FY modes of tribofilms formed by transmission oils.

* yoshimu.iwanami@eneos.co.jp

7A /2001G013

Depth-resolved XMCD study on Fe/Cu(001)

Soichiro KITAGAWA[1], Kenta AMEMIYA[1*], Daiju MATSUMURA[1], Toshihiko YOKOYAMA[2], and Toshiaki OHTA[1]

[1]Department of Chemistry, Grad. School of Science, The Univ. of Tokyo,
7-3-1 Hongo, Bunkyo-ku, Tokyo 113-0033

[2] Institute for Molecular Science, Myodaiji-cho, Okazaki, Aichi 444-8585, Japan

Introduction

Fe/Cu(001) ultrathin film is one of the most widely investigated systems because of the large variety of its structural and magnetic properties that depend on the Fe film thickness. Between 5 to 10ML, it takes a fcc structure with reconstructed surface fct layers. The surface 2 layers are known to be ferromagnetic (out-of-plane) [1], while the inner layers are either anti-ferromagnetic or in a SDW (spin-density-wave) state [2].

In this report, we have developed a novel depth-resolved XMCD (x-ray magnetic circular dichroism) method and applied to this system to clarify the magnetic structures of this system.

Experimental

Cu(001) single crystal was cleaned by repeated cycles of Ar^+ sputtering and annealing to 900K. Fe was deposited by an e-bombardment heating of Fe-rod, and the film thickness was monitored by *in situ* RHEED observation. The sample was cooled down to 110K and magnetized perpendicular to the film surface by a pulsed current through a coil.

All the XMCD experiments were performed at BL-7A. Circularly polarized x-rays were obtained by using x-rays emitted above (or below) the electron orbit plane of the storage ring by 4mrad ($P_C \approx 0.8$). For the depth-resolved XMCD measurement, a slit was mounted above the microchannel plate (MCP) to count the electrons emitted only along the detection angle θ_d. The acceptance angle of MCP was 5° (see inset of Fig. 1).

Results and discussion

Fe-L XMCD spectra for the 8ML Fe film were measured at detection angles θ_d =0, 4, 8,12, and 15°. We also estimated the probing depth λ for each θ_d by the Fe-L edge jump height (@740eV) of each θ_d as a function of the film thickness. A self-absorption effect of x-rays was also taken into account. Estimated probing depth λ ranges from 2.1*d* to 3.9*d* depending on θ_d. (Note that *d* denotes the interlayer distance of the Fe film.)

The XMCD spectrum measured at a certain detection angle is the sum of contribution from each layer weighted by an exponential decay function of the depth. Thus we can, in principle, extract the XMCD spectra corresponding to each single layer. However, as for the 8ML film, we divided the film into two regions of different magnetic property; the surface two layers and the rest inner 6 layers. Then we assumed that the magnetic structure of the inner layers is in a SDW state and the SDW wave number is optimised as a parameter. Note that this assumption covers collinear anti-ferromagnetic states and non-magnetic states as the extreme cases. The fitting is optimised when the wave number $q=2\pi/2.4d$. The collinear anti-ferromagnetic states ($q=2\pi/2d$)is unlikely to be adopted. The magnetic structure obtained by the fitting result is shown in Fig.2.

[1] M.Straub et al., PRL 77(1996) 743
[2] D.Qian et al., PRL 87(2001) 227104

* amemiya@chem.s.u-tokyo.ac.jp

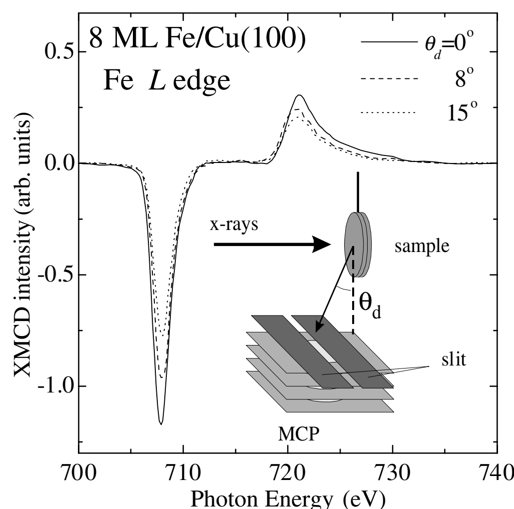

Fig.1 The setup of depthresolved XMCD and obtained spectra

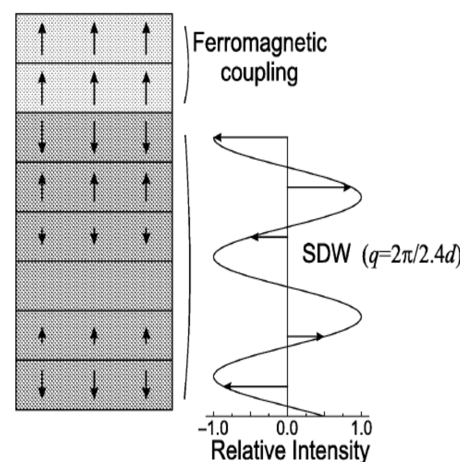

Fig.2 Schematic magnetic depth profile of the 8ML Fe film.

3B,16B/2001G021

Si $L_{2,3}$ emission spectra from the interfaces in antiferromagnetically coupled Fe/Si multilayers II

Takashi IMAZONO,* Yushi HIRAYAMA, Noboru MIYATA, Osamu KITAKAMI, and Mihiro YANAGIHARA
Institute of Multidisciplinary Research for Advanced Materials, Tohoku University, Sendai 980-8577

Introduction

The Fe/Si multilayer has been widely studied for the strong antiferromagnetic coupling between the Fe layers. However, the models so far proposed for the origin are controversial because of the severe interdiffusion at the interfaces. Endo *et al.* [1] studied the interlayer coupling for a series of $Fe/Fe_{1-x}Si_x$ ($0.4 \le x \le 1.0$) multilayers deposited at a high rate and explained the results qualitatively by the quantum-well model rather than the RKKY model. Besides, they observed the strongest interlayer coupling for the Fe/Si(1.3nm) multilayer among the Fe/Si(t) multilayer series. However, the origin of the enhancement was not yet understood because the material of the mediating layer was not assigned. In the previous study [2] we investigated using soft X-ray emission (SXE) spectroscopy the interface of the Fe/Si(t) multilayers whose magnetic and electric properties were confirmed by Endo *et al.* The result suggested that there should remain a thin layer of high resistive Fe-Si alloy or *a*-Si sandwiched between the Fe_3Si layers. However, the mediating material was not assigned in that study. In this study we remeasured the SXE spectra for the Fe/Si(t) multilayers at high-flux beamlines.

Experimental

The Fe/Si(t) multilayers were grown to 22 bilayers on Si substrates with the thickness of the Fe layer fixed at 3.0 nm and the thickness t of the Si layer using a dc magnetron sputter system. The SXE experiments were carried out at BL-3B and 16B using an SXE spectrometer of a flat-field type. The resolution of the spectrometer was about 0.5 eV at 100 eV.

Results and discussion

Figure 1 shows the Si $L_{2,3}$ emission spectra measured for the Fe/Si(t) multilayers of t = 0.5, 1.0, 1.3, 1.5, 1.7, 2.0, and 3.0 nm and amorphous Si (*a*-Si) excited at 120 eV. The spectrum of the Fe/Si(3.0 nm) multilayer is very similar to that for *a*-Si, which suggests that the Si layer almost consists of *a*-Si. The spectrum changes with decreasing t, which suggests that the interface region of the Fe/Si(t) multilayers almost consists of Fe-Si alloys rather than *a*-Si. The effective thickness of the alloys was estimated by reproducing the Si $L_{2,3}$ spectra of the multilayers using those of Fe_3Si, FeSi, $FeSi_2$, and *a*-Si. Figure 2 shows their thickness as a function of t. For the Fe/Si(1.3nm) multilayer Fe_3Si, $FeSi_2$, and FeSi are dominantly observed but not *a*-Si. This result means that the contribution of *a*-Si to the magnetic interlayer coupling is negligible. Fe_3Si is also excluded from the materials to mediate the interlayer coupling because it is ferromagnetic. Thus $FeSi_2$ plays an important role in the antiferromagnetic coupling in the Fe/Si multilayer. The effective thickness for $FeSi_2$ is about 0.7 nm.

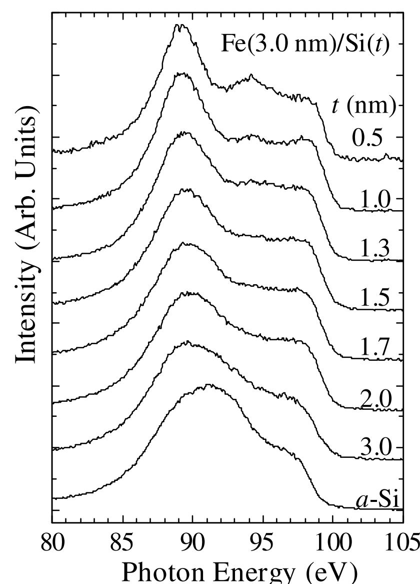

Fig. 1. Si $L_{2,3}$ SXE spectra of the Fe/Si(t) multilayers of t = 0.5, 1.0, 1.3, 1.5, 1.7, 2.0, and 3.0 nm and *a*-Si.

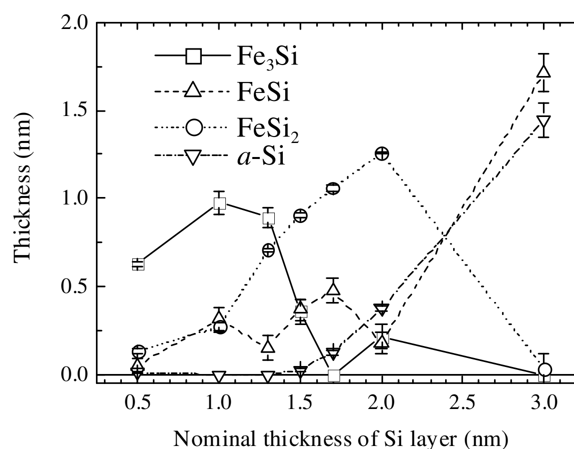

Fig. 2. Thickness of Fe_3Si, FeSi, $FeSi_2$, and *a*-Si estimated for the interlayer.

References

[1] Y. Endo *et al.*, Phys. Rev. B**59**, 4279 (1999).
[2] T. Imazono *et al.*, PF Activity Report 2000 Part B p.42.

* imazono@rism.tohoku.ac.jp

14A/2001G045

Grading effects in X-ray specular reflectivity analysis

Mari MIZUSAWA and Kenji SAKURAI*
National Institute for Materials Science, Sengen, Tsukuba, Ibaraki 305-0047, Japan

Introduction

Grazing incidence X-ray reflectometry is a powerful tool for surface analysis [1,2]. Specular reflectivity permits the analysis of density profile and roughness. However, our recent experiments [3] at BL14A have revealed the significance of considering grading at the surface and interfaces. Conventional models based on stacking uniform layers with interface roughness can sometimes lead to the wrong conclusion. This report describes some calculations.

Results and Discussion

Calculations were based on Parratt's theory [4] and assumed that the density gradient can be treated as a multilayered structure composed of extremely thin slices with different densities. Fig.1 shows the results for synthtic quartz substrate, the surface of which has linear and Gaussian grading, respectively, in the top 2 nm region. It is possible to analyze the reflectivity curve obtained by conventional procedures, i.e., curve fitting to the model taking into consideration homogenous layers and interface roughness. In this case, it was necessary to assume 2 thin layers on the substrate (i.e., 3-layer model) in order to obtain a good fit. The obtained parameters are summarized in Table 1. The corresponding reflectivity curves are plotted as dashed lines in Fig.1 as well.

The fit is quite good, and the differences in the reflectivity curves are small. However, one can see that the density for the 2nd intermediate layer is high for both grading cases, and even higher than that of the bulk (2.65 g/cm^3). Also, the roughness of the interface between the 1st and 2nd layers is quite big compared with other interfaces. Those unnatural features frequently appear when analysing practical samples, which usually have some grading due to chemical diffusion and/or near-surface damages during polishing etc. Even so, the present calculation requires further extension. It is probably not practical to treat roughness simply as a part of the density gradient

References

[1] J.Daillant, A.Gibaud, "X-Ray and Neutron Reflectivity: Principles and Applications", Springer,(1999).
[2] M.Tolan, "X-Ray Scattering from Soft-Matter Thin Films", Springer, (1999).
[3] M. Mizusawa and K.Sakurai, this report
[4] L.G.Parratt, Phys. Rev., 95, 359, 1954.

*sakurai@yuhgiri.nims.go.jp

Table 1. The parameters obtained by the model neglecting grading effects for synthetic quartz

	Linear grading			Gaussian grading		
	Thickness (nm)	Roughness (nm)	Density (g/cm^3)	Thickness (nm)	Roughness (nm)	Density (g/cm^3)
Layer 1	1.24	0.10	0.93	1.56	0.1	0.93
Layer 2	1.07	0.83	2.95	0.56	0.39	3.13
Substrate	-	0.21	2.65	-	0.21	2.65
R value	Normal	1.56×10^{-6}		Normal	1.87×10^{-7}	
	Log	9.51×10^{-5}		Log	1.35×10^{-4}	

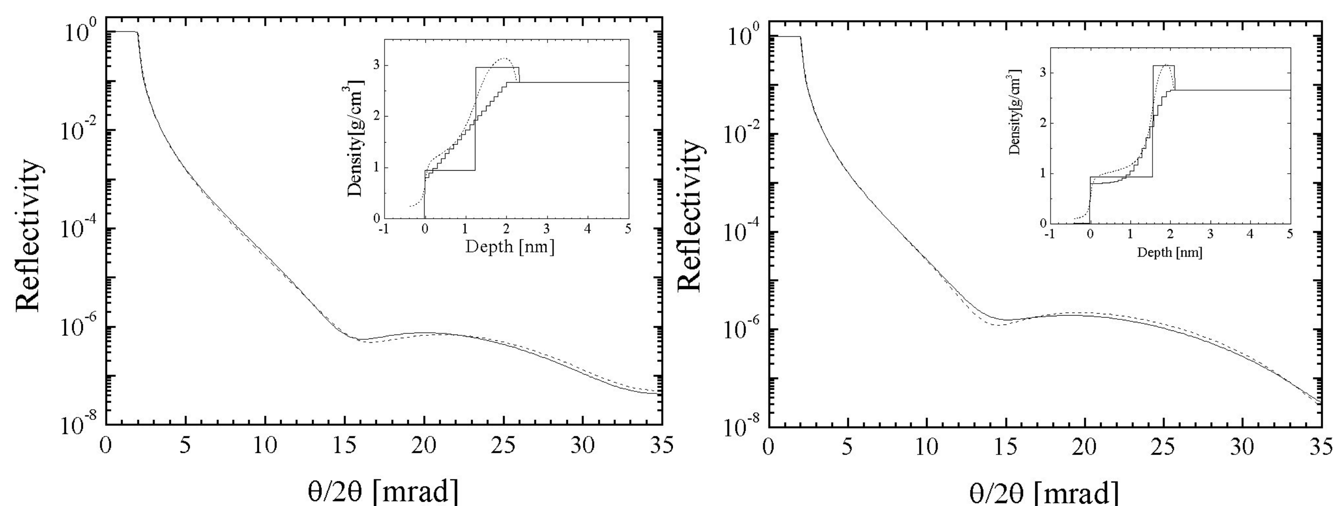

Figure 1. Calculated results for synthetic quartz with graded surface using a density grading model (solid line) and fitting results using a model with 3 homogeneous layers (dashed line). The models are shown as insets (the dashed line is the electron density profile obtained from the fitting to the 3-layer model). Linear grading c (left), Gaussian grading (right). The fitting results are shown in Table 1.

14A/2001G045

Grazing-incidence diffuse scattering for Ni/C multilayers

Shuichiro KUWAJIMA[1], Hisataka TAKENAKA[2] and Kenji SAKURAI[1*]
[1]National Institute for Materials Science, Sengen, Tsukuba, Ibaraki 305-0047, Japan
[2]NTT Advanced Technology Corporation, Tokai, Ibaraki 319-1193, Japan

Introduction

The Ni/C multilayer is one of the most useful optical mirrors for soft X-rays [1,2]. It is significant in the investigation of interfaces because the preparation of a perfect layer-stacking structure is crucial to obtaining high reflectivity. In this study, diffuse scattering around the Bragg condition was measured.

Experimental

The sample measured is $[Ni(16.6Å)/C(18.8Å)]_{100}$ (2d=70.8Å) deposited on a silicon substrate, prepared by sputtering. The experiment was carried out with 16keV monochromatic X-rays. Details of the grazing incidence X-ray reflectometer can be found elsewhere [2].

Results and Discussion

Fig. 1 shows a typical 2D rocking scan around the 1st Bragg peak (11.26 mrad), which was performed by scanning glancing angle θ_i for a fixed scattering angle series ($\theta_i+\theta_f$). While a strong Bragg reflection peak with many fringes is visible as a specular reflectivity curve, one can see that diffuse scattering also becomes strong at the same scattering angle at around 22.5 mrad (qz =1.83 nm^{-1}). This is due to the strong correlation with the interface roughness, and such enhancement has sometimes been reported for a Ni/C multilayer [2]. Preliminary analysis indicates that both the rocking curves (qx scan) and longitudinal curves (qz component of 2D scan) obtained at the off-Bragg condition appear rather close to Lorenzian. Fig 2 shows the full width at the half maxima (FWHM) of the rocking curves as a function of qz. It is approximately proportional to qz^2, except for some oscillation around the Bragg condition. Those results indicate a certain typical Fractal morphology, corresponding to a Hurst parameter of around 0.5 [4]. The authors would like to thank Prof. S. Kishimoto for his kind assistance during the experiment.

References

[1] H. Takenaka *et al.*, Thin Solid Films, 288, 99 (1996).
[2] B.K.Tanner and J.M.Hudson, IEEE MAG 28, 2736 (1992).
[3] K. Sakurai *et al.*, J. Synchrotron Rad. 5, 554 (1998).
[4] M.Tolan, "X-Ray Scattering from Soft-Matter Thin Films", Springer, (1999).
*sakurai@yuhgiri.nims.go.jp

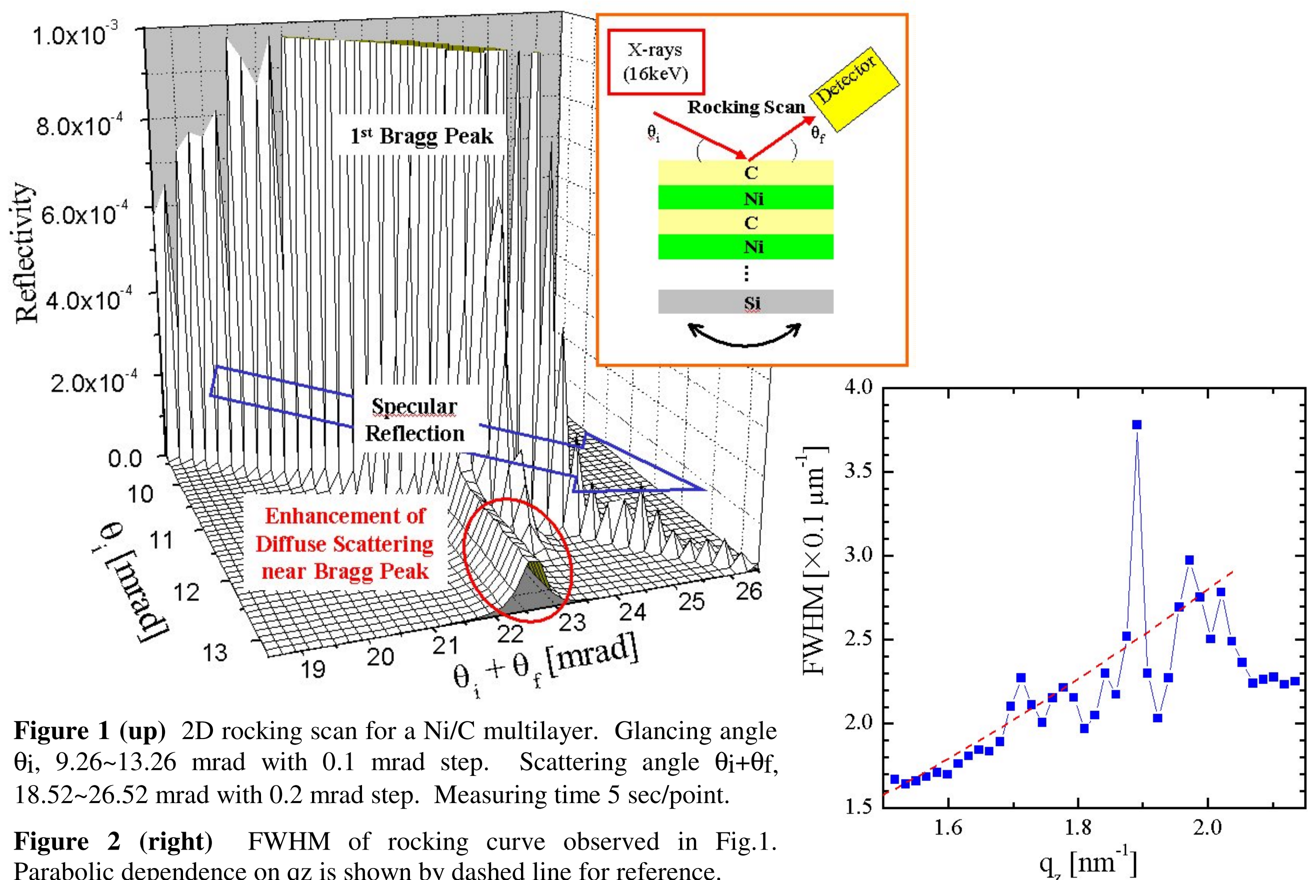

Figure 1 (up) 2D rocking scan for a Ni/C multilayer. Glancing angle θ_i, 9.26~13.26 mrad with 0.1 mrad step. Scattering angle $\theta_i+\theta_f$, 18.52~26.52 mrad with 0.2 mrad step. Measuring time 5 sec/point.

Figure 2 (right) FWHM of rocking curve observed in Fig.1. Parabolic dependence on qz is shown by dashed line for reference.

14A/2001G045

Grazing-incidence X-ray specular reflectivity study on a rutile (110) surface

Mari MIZUSAWA and Kenji SAKURAI*
National Institute for Materials Science, Sengen, Tsukuba, Ibaraki 305-0047, Japan

Introduction

Fine rutile (TiO_2) powder is one of the most promising materials for future solar cell applications. Since the powder's electronic properties depend highly on the degree of preferred <110> orientation, studying a single crystal (110) surface in a realistic environment is significant [1]. In this study, grazing incidence X-ray scattering has been employed to observe the annealing effect.

Experimental

The samples measured are mirror-polished rutile (110) single crystal substrates that are commercially available (Nakazumi). The surface has been cleaned in a dilute HNO_3 bath (10vol%, 100°C, 15min). Sample A is as cleaned, and sample B is annealed at 300°C for 1 h in a vacuum (10^{-3}Pa) after HNO_3 cleaning. The colour of sample B did not change after annealing. The experiment was carried out with 16keV monochromatic X-rays.

Results and Discussion

Figure 1 shows the specular reflectivity with 8.5 decades for the rutile (110) surfaces, A and B. The critical angle is 2.45 mrad, indicating that the density is around 4.26g/cm^3, which agrees well with that for solid bulk rutile. The slow oscillation observed at 10~28mrad indicates some density gradient at the near surface. Calculations have been made based on Parratt's model assuming thin surface layers with different density and thickness. The calculated reflectivity curves show good agreement with the experimental results.

Proposed models for the sample A and B are shown in Figure 2. They have an interesting density profile, i.e,, (i) an extremely low density layer (0~10 Å, density ~1), which could correspond to some adsorption, (ii) a moderately low density layer (15~30 Å, density 2.77~4.26), which is probably due to some near-surface damage caused by polishing and (iii) a transition region (10~15 Å). In the early stage of analysis, we obtained a good fit for the 2 thin layers model, shown as a dashed line in Figure 1. The model was not adopted because it was concluded that the density for the 2nd layer is 3~6 % higher than the bulk, which can not be explained reasonably. However, it definitely suggested a remarkable density contrast in the near-surface region, and the profile proposed in Figure 2 interprets this well. One should note that sample B has a lower density than A because of annealing. The averages for the whole surface layers are 2.55 and 2.37, for A and B, respectively; the averages for the moderately low density layers are 3.43 and 3.34, for A and B, respectively.

Another comparison between A and B can be discussed in terms of their surface morphologies. The diffuse scattering measurements performed for these samples did not show that great a difference, but the rather weak intensity of sample B could indicate that annealing can contribute to some flattening of the surface. The authors would like to thank Prof. S. Kishimoto and Dr. S. Kuwajima for their kind assistance during the experiment.

References

[1] P.A.M. Hostenpiller et al, J. Phys. Chem. B, **102**, 3216 (1998)

*sakurai@yuhgiri.nims.go.jp

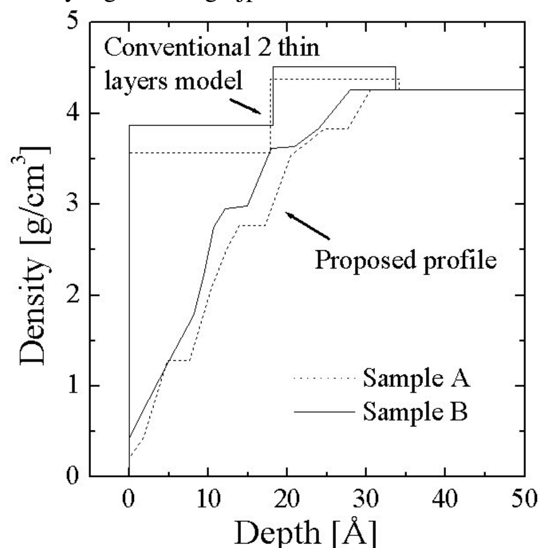

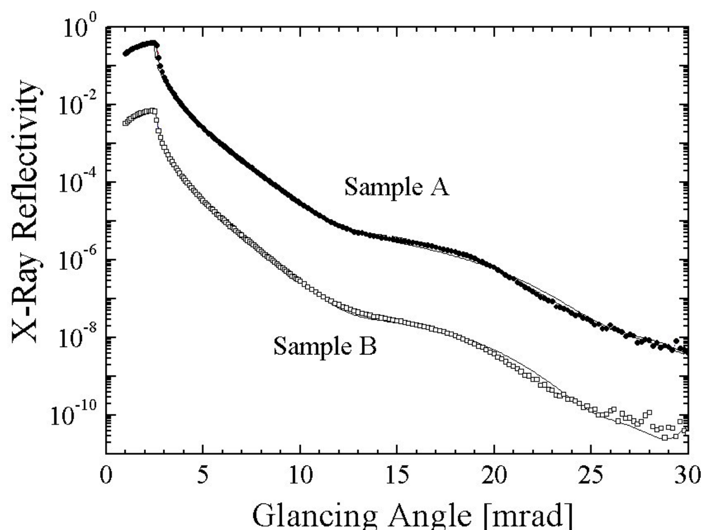

Figure 1 (left) Specular reflectivity for sample A (squares), and B (circles). The curve-fitting results are shown with solid lines (density gradient density model) and dashed lines (2 thin layers model).
Figure 2 (up) Proposed surface density profile.

9C, 14B, 15C/2001G055

Study of α-Al_2O_3/Ru(0001) structure by X-ray diffraction

Shinichiro NAKATANI*[1], Toshio TAKAHASHI[1],
Kazuo NAGATA [2], Wataru YASHIRO [3] and Yoshitada MURATA [2]
[1]Institute for Solid State Physics, The University of Tokyo
Kashiwanoha, Kashiwa, Chiba 277-8581, Japan
[2]Physics Department, The University of Electro-Communications
Chofugaoka, Chofu, Tokyo 182-8585, Japan
[2]National Institute of Advanced Industrial Science and Technology
Higashi, Tsukuba, Ibaraki 305-8565, Japan

Introduction

Single-crystal oxide films are important materials from standpoints of fundamental research and application. Those materials are expected to show interesting properties, such as band gap narrowing and metal-insulator transition, when they are grown on metallic crystal surfaces[1]. Since those electronic properties are dependent on the thickness and the quality of the crystal oxide film, characterization of the film by X-rays is required. Synchrotron radiation is necessary for the characterization because the thickness of the film is so thin, about 10 Å, that the expected intensity of X-rays reflected from the film is very weak. In this work, we examine α-Al_2O_3/Ru(0001), which has various potentials for application in thin-film technology[1,2].

Experimental

The combination of α-Al_2O_3 and Ru is very convenient for crystal growth because of the small mismatch between their lattice constants.

Our sample was prepared in an ultrahigh vacuum chamber. A disk of Ru(0001) single crystal was set in the chamber and its surface was cleaned by annealing. Al was deposited on the clean surface from a tungsten basket. After the deposition, a crystalline film of α-Al_2O_3 was grown by heating the surface in O_2 atmosphere. The designed thickness of the α-Al_2O_3 film is 15 Å.

The experiment was performed at BL-9C using a 6-axis diffractometer controlled by SPEC. X-rays of wavelength 1.0 Å were selected by a double-crystal monochromator and focused by a bent-cylindrical mirror. The contamination of the higher harmonics was removed by the mirror. The intensity of reflected x-rays was measured along the 00 rod.

Results and discussion

The result of the measurement is shown in Fig.1. The strong reflection at L=2 is caused by the Bragg reflection of the Ru substrate. It is not clear what weak reflections at L=1 and L=3 are attributable to, since that L is odd is the cancellation condition for not only Ru but also α-Al_2O_3. One remarkable feature of the reflection curve is the fluctuation of intensity around L=1. If this fluctuation is caused by interference of x-rays reflected from the Ru substrate and the α-Al_2O_3 film, it could be a key to evaluate the thickness of the film. Now we are making preparations for the further experiment.

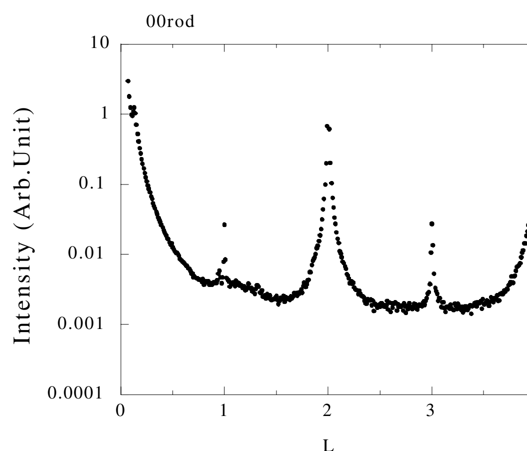

Fig.1. Intensity of reflected x-rays measured along the 00 rod.

References

[1] Y.Murata et al., J. Phys. Soc. Jpn. **70** 793 (2001). and references there in.
[2] B.G Frederick et al., Surf. Sci. **244**, 67 (1991).

*nakatani@issp.u-tokyo.ac.jp

9C,14B, 15C/2001G065

Characterization of a-Si/Fe/Si(111) interface by X-ray standing wave

Shinichiro NAKATANI*[1], Keisuke SHIMIZU[1], Toshio TAKAHASHI[1] and Keiichi HIRANO[2]
[1]Institute for Solid State Physics, The University of Tokyo
Kashiwanoha, Kashiwa, Chiba 277-8581, Japan
[2]Institute of Materials Structure Science, KEK-PF, High Energy Accelerator
Research Organization
Oho-machi, Tukuba, Ibaraki 305-0801, Japan

Introduction

Iron films deposited on Si(111)7x7 surfaces form various structures according as the deposition thickness changes. Those structures are interesting subjects of X-ray study because their atomic arrangements are not determined. We applied X-ray standing wave (XSW) method to investigation of an a-Si/Fe/Si(111) sample. This method has two merits: firstly, it can investigate buried interface structures non-destructively and secondly, its spatial resolution is very fine since it makes use of the interference fringes of x-rays as a scale

Experimental

Our sample was prepared in the following way. First, about 1ML of Fe was deposited onto a Si(111) substrate by an effusion cell at room temperature and the substrate was annealed at 500°C. After the annealing, the 2x2 RHEED pattern was observed as shown in Fig.1. Finally an a-Si cap layer of 90 Å was deposited to keep the 2x2 structure intact.

The X-ray measurement was performed using synchrotron radiation from a vertical wiggler of BL-14B. The geometry of the measurement is the (+,-) parallel setting of 111 reflection. X-rays of wavelength 1.2 Å were selected by a double-crystal monochromator. The X-rays were reflected by a Si(111) fore crystal and the Si(111) substrate subsequently in the experimental hutch. The intensity curve of the X-rays reflected from the sample (rocking curve) and the yield curve of fluorescent X-rays of FeKα were measured by a PIN detector and an SSD, respectively, around the 111 Bragg point

Results and discussion

The rocking curve and the yield of FeK fluorescence are shown in Fig.2. The profile of the measured rocking curve is slightly narrower than the theoretical curve probably because of the non-linearity of the PIN detector. The fluorescence yield curve, which indicates the interaction between the XSW field and Fe atoms, shows an almost symmetrical form. This means that Fe atoms diffuse at the interface and do not stay on any particular sites. Improvement of sample preparation is necessary for further study.

Fig.1. RHEED pattern observed along the silicon [112] azimuth.

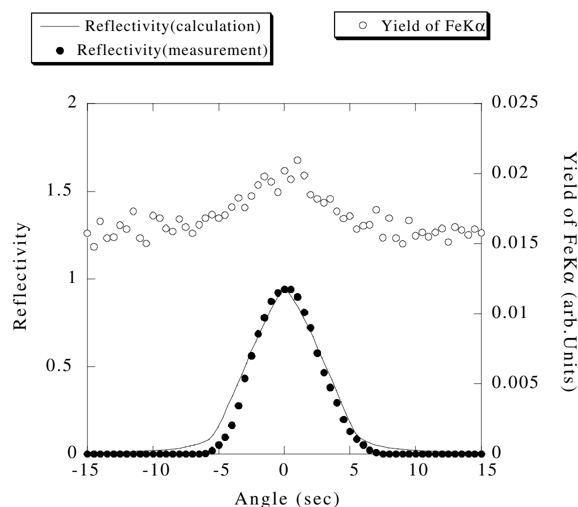

Fig.2. Rocking curve of the 111 reflection and yield of FeK fluorescence

*nakatani@issp.u-tokyo.ac.jp

13C/2001G108

Carbon K-edge x-ray absorption spectroscopic analysis of photo-degraded polyimide film

Tomoaki TANAKA*[1, 2], Kyoko K. BANDO[1], Nobuyuki MATSUBAYASHI[1], Motoyasu IMAMURA[1], Hiromichi SHIMADA[1]
[1]National Institute of Advanced Industrial Science and Technology, Tsukuba, Ibaraki 305-8565, Japan
[2]New Energy and Industrial Technology Development Organization, Toshima-ku, Tokyo 170-6028, Japan

Introduction

The environmental modification of polyimide film is with considerable industrial interests. Pyromellitimido-oxydianiline (PMDA-ODA) polyimide (PI), known as Kapton films, have widely been used in many industries due to the excellent physical and thermal properties. One of the recent applications of the PMDA-ODA PI film has been found in the aerospace industry as thermal blankets. In this situation, the polyimide films are exposed to the aerospace environment and thus damaged by strong UV irradiation. The purpose of the present study is to elucidate the structural changes of PMDA-ODA PI films when exposed to the strong UV irradiation. For this purpose, we have prepared PMDA-ODA PI films exposed to an UV light source and analyzed the structural changes by using x-ray absorption spectroscopy (XAS).

Experimental

The carbon K-edge XAS measurements were performed at the BL-13C with the partial electron yield (PEY) method using a micro-channel-plate (MCP). Our XAS measurement system can overcome the problem of charging of sample surface using an electron flood gun that can supply a large current of low energy electrons to the sample surface [1]. The XAS spectrum was obtained by dividing the PEY signals by *Io* intensity that was separately acquired by measuring the total electron yield from a sputtered Au plate. This is quite important because the *Io* profile exhibited a large intensity modulation at the carbon K-edge region due to the carbon contamination on the beam line optics. The polyimide films analyzed were non-irradiated and UV irradiated PMDA-ODA PI films for 10, 30 and 60 minutes with a diameter of 5 mm and a thickness of 10 m. A low-pressure mercury lamp was used as the UV light source.

Results and discussion

Figure 1 indicates a unit structure of PMDA-ODA PI that consists of PMDA and ODA subunits. The carbon K-edge XAS spectra of the PMDA-ODA PI film are shown in figure 2. Each peak of the carbon K-edge XAS spectrum is interpreted as transitions from C1s to the π^*(C=C, C=O), σ^*(C-O, C-N, C=C) resonance for the PMDA and ODA subunits. The assignments of these transitions described in Table 1 were done based on a report [2] and shown in Fig.

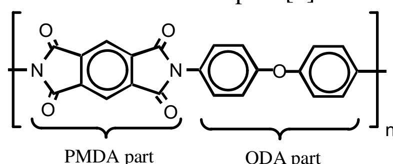

Figure 1 Unit structure of PMDA-ODA PI films

2. All the σ* and π* features from the aromatic ring carbons of the PMDA and ODA unit decreased with increasing the UV irradiation time. These observations suggest that the UV irradiation broke some bonding and produced new bonding that resulted in the degradation of the ordered PMDA-ODA structure. The intensity of the π* feature assigned to the transition to C=O in the imide group of PMDA unit most significantly decreased. It is very likely that the PMDA ring was selectively cleaved, whereas relatively small change took place in the ODA unit. At the same time, the intensity of a new peak at 288.1 eV increased with increasing the UV irradiation time.

According to building block approach, this peak can be assigned to a carboxyl group. We find that the UV irradiation caused cleavage of imide rings of PMDA units that resulted in the formation of carboxyl groups. Further study is needed to conclude the structural changes caused by UV irradiation.

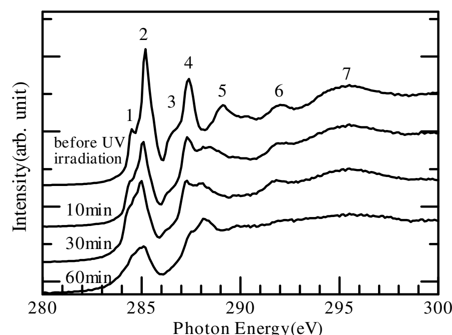

Figure 2 C K-edge XAS spectra of PMDA-ODA PI film; before UV irradiation, UV irradiation of 10, 30 and 60min

Table 1 Assignments and positions of polyimide film of PMDA-ODA type

	Peak (eV)	Ref.[2]	Assignment
1	284.5	284.8	π*(C=C) (PMDA)
2	285.2	285.2	π*(C=C) (ODA)
3	286.41	286.6	π*(C=C) (ODA)
4	285.7	287.4	π*(C=O)
5	289.4	289.2	π*(C=C) (PMDA, ODA)
6	292.2	291.9	σ*(C-O, C-N)
7	295.6	295.4	σ*(C=C) (ODA)

References

[1] T. Tanaka et al., J. Electron Spectrosc. Relat. Phenom. **114-116**, 1077(2001).
[2] J. L. Jordan-sweet et al., J. Chem. Phys., **89**, 2482 (1988).

* tanaka-t@aist.go.jp

10B/2001G128

Anomalous redox properties of copper-ion-exchanged ZSM-5 prepared by microwave- assisted method

Takae OKAMOTO, Atsushi ITADANI, Ryotaro KUMASHIRO, Masatoshi MARUKI, Hideo ONISHI, Yasushige KURODA, Yuzo YOSHIKAWA, and Mahiko NAGAO*
Okayama University, Tsushima-naka, Okayama 700-8530, Japan.

Introduction

It is widely recognized that copper ion-exchanged ZSM-5-type zeolite (CuZSM-5) exhibits a high catalytic activity in the direct NO*x* decomposition into N_2 as well as a pronounced adsorption property at room temperature for N_2 molecule. In both phenomena, there is fairly general agreement that the active center is the monovalent copper ion formed in the evacuation process. However, the states of copper ion exchanged are different depending on the conditions used in the preparation procedures, i.e., pH of solution, kind of counter ions, exchanging methods, temperatures adopted in the ion-exchange procedure, and so on. We have recently found that the CuZSM-5 sample prepared by utilizing microwave power has a prominent redox feature. In this report, we have inclined to know the reduction and oxidation behaviors of the copper ion in CuZSM-5 exchanged by different methods. From the viewpoints of controlling the properties of zeolite arbitrarily, it is important to clarify the influence of ion-exchange methods on the properties of copper ion and of the state of mother zeolite on the state of exchanged ion.

Results and discussion

Figure 1 shows the copper K-edge EXAFS and XANES spectra for the CuZSM-5(CM)-108 sample prepared by utilizing microwave power in an aqueous solution of $CuCl_2$, where the value, 108, represents the ion-exchange capacity in percent and the terms C and M mean chloride ion and microwave used. The sample had been evacuated at increasing temperatures in the region of 300–873 K. The first band centered at 1.52 Å (no phase-shift correction) in EXAFS spectra is attributed to the back-scattering from the nearest neighboring skeletal oxygen atoms and the resulting coordination number is estimated to be *ca.* 2.5 for the 873 K-treated sample through the least-square method by using Cu_2O as a reference substance. The prominent feature is observed in the spectra for the samples treated at above 673 K: the appearance of the distinct, new, and fairly strong band at around 2.12 Å. This band can be assigned to one due to the back-scattering from the first nearest metal species, by comparing with the spectrum for reference copper metal; the metal formation is clearly evidenced.

With reference to the XANES spectra, the weak shoulder at 8.978 keV observed for the sample which was evacuated at 300 K is attributable to the 1s-3d transition, indicating that the copper ion exchanged in the sample takes a divalent state. Successive pretreatments at the higher temperatures bring about strong and specific bands at 8.983 and 8.995 keV which are assigned to the 1s-4p and 1s-4p transitions in the monovalent copper ion (Cu^+), respectively. The appearance of such two sharp bands suggests that this Cu^+ species takes either linear or planar configuration but not tetrahedral one. The 673 K-treatment brings about a broadening of the band at around 8.983 keV, accompanying a shoulder at lower side of this band and a new and weak band at 9.005 keV. By comparing with the spectrum of reference metal, the formation of metal species is also suggested. Further treatment at higher temperatures leads to more distinct band feature specific to the metal species, coinciding with the results obtained by EXAFS measurements. These data clearly prove that the evacuation procedure of the CuZSM-5(CM)-108 easily produces small metal clusters in zeolite.

Included in Figure 2 for comparison are EXAFS and XANES spectra for the CuZSM-5(C)-120 sample which was traditionally prepared at 363 K by using an aqueous solution of $CuCl_2$. As is distinct from the spectra shown in Figure 1, it is clearly evidenced that the bands being ascribable to the metal species were not observed in both EXAFS and XANES spectra.

In addition, ESR spectrum of the sample treated at above 673 K for CuZSM-5(CM) gave a new and sharp band at a *g* value of 2.002, which can be assigned to the free electron trapped in the defect site, accompanied with the extremely weak bands due to the divalent copper species. On the other hand, this new band was not observed for the 673 K-treated CuZSM-5(C) sample.

As a result, it has also become apparent that each sample shows different propensities for reducibility from the divalent copper ion to the monovalent or zerovalent one; 673 K-treatment of the CuZSM-5(CM)-108 sample results in a drastic increase in the band intensity at 2.12 Å and the appearance of a shoulder band at around 8.983 keV, whereas the CuZSM-5(C)-120 sample scarcely exhibits both bands. These facts can be interpreted as follows: the formation of the defect sites due to the poor crystallinity of the sample, which was assisted in the ion-exchange process with microwave-assisted method, is a dominant factor in the reducibility of Cu^{2+} to zerovalent species.

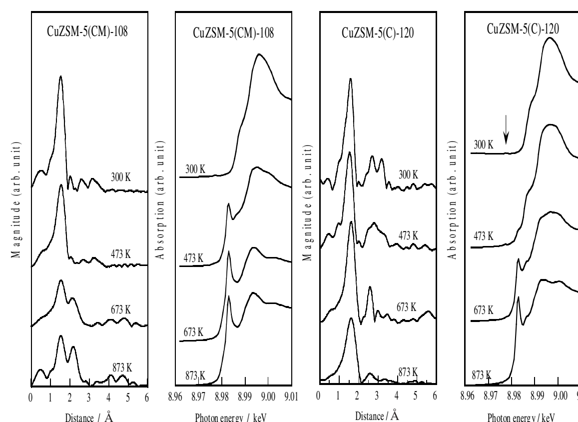

Figures 1 and 2 EXAFS and XANES spectra.

*mnagao@cc.okayama-u.ac.jp

11B/2001G312

Surface chemical imaging of energy filtered photoemission electron microscopy (EXPEEM)

Hideyuki YASUFUKU[1†], Yusuke OHMINAMI[1], Tetsuya TSUTSUMI[1], Kiyotaka ASAKURA*[1], Yoshiyuki KITAJIMA[2],Makoto KATO[3], Yuji SAKAI[3] and Yasuhiro IWASAWA[4]
[1] CRC, Hokkaido University Sapporo 060-0811, Japan
[2] Photon Factory, Institute of Material Structure Science,Oho 1-1, Tsukuba 305-0811, Japan
[3] JEOL Ltd, 3-1-2 Musashino, Akishima, Tokyo 196-8558, Tokyo 113-0033, Japan
[4] Department of Chemistry, Graduate School of Science, The University of Tokyo, Hongo, Bunkyo-ku, Tokyo 113-0033, Japan

Introduction

Surface chemical imaging is one of the important techniques to investigate the surface chemical processes. We can successfully obtain chemical surface imaging of of Au islands on a Ta sheet by means of energy-filtered photoemission electron microscopy (EXPEEM).

Experimental

Figure 1 is a sketch of the EXPEEM system used in this study. The sample is biased at –10 kV against the objective lens which is grounded. The accelerated photoelectrons go through the objective lens, intermediate lens and then arrive at the Wien filter. In the Wien filter, magnetic field and electric field are perpendicularly applied. Thus only the electrons satisfying the $\vec{E} = \vec{v} \times \vec{B}$ travel straightly through the Wien filter and give the surface images. By choosing kinetic energies characteristic to the elements, the image reflects their distribution.

The Au was evaporated in vacuum on the Ta sheet through the Ni mesh with 10 m square opening in a 25 m period. The thickness of the Au islands are 1 µm.

EXPEEM instrument was installed at BL11B and the X-ray energy was fixed at 2300 eV which was just above the Au M_4 edge.

Results and discussion

Fig.2 shows the EXPEEM image of Au islands on the Ta sheet using electrons with various kinetic energies. Fig.2a is the image with the secondary electrons with kinetic energy = 0eV. Because the X-ray energy is just above the Au M_4 edge, the Au islands are brighter than the Ta substrate. When the higher kinetic energies of photoelectrons are selected to pass the Wien filter, the brightness of the image decreased a lot because the decrease of the amount of secondary electrons. Fig. 2b shows the image using electrons with kinetic energies of 60 eV which was just below the Au $3d_{5/2}$ photoelectron peaks. Au gives the brighter image due to the inelastic electrons of Au 3d photoelectron peak. Fig.2c is the image of electrons with the kinetic energy at 102 eV just at the energies of Ta 3p photoelectrons where we had a brighter Ta image. Spatial resolution was 2 m and energy resolution was 15 eV. Fig. 2d shows the image of electrons with their kinetic energies at 112 eV. The contrast became worse and Au islands were hardly identified. Thus the image contrast shown in Fig.2c reflected the $Ta_{3/2}$ photoelectron kinetic energies and element distribution. As far as we know this is the first surface chemical photoelectron imaging using a high energy X-ay with a spatial resolution of 2 m.

*askr@cat.hokudai.ac.jp
†Present address: Advanced Materials Laboratory, National Institute for Materials Science, BL15 Spring-8, Mikazuki, Hyogo 679-5198, Japan

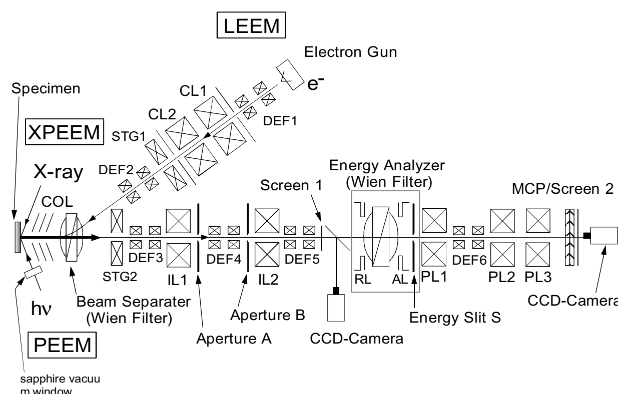

Figure 1. Sketch of the EXPEEM system with a retarding Wien-filter.

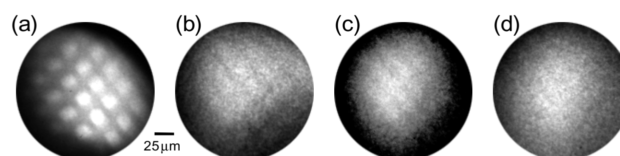

Figure 2. Energy-filtered XPEEM images of Au on Ta substrate. Kinetic energy =0 eV(a), 60 eV(b),102 eV (c) and 112 eV(d). The photon energy was 2300 eV. The photoelectron energy of (c) corresponds to Ta $3p_{3/2}$.

27A/2001G334

Core level spectroscopy study for cluster-like Si deposited on graphite and insulating sapphire

Krishna G. NATH *, Iwao SHIMOYAMA, Tetsuhiro SEKIGUCHI and Yuji BABA
Synchrotron Radiation Research Center, Japan Atomic Energy Research Institute,
Tokai-mura, Naka-gun, Ibaraki 319-1195, Japan

In the coming nanotechnology age, Si-assembled nanostructures will be the key components for fabrication of many nanodevices. Due to technological and research importance, study of Si-epitaxy on inert substrates, such as semi-metallic graphite [1] and insulating sapphire [2] has attracted much attention in recent years. For example, scanning tunneling microscopy measurement was performed to observe the Si nanowires on graphite [1]. However, electronic structures of Si nanowires and Si-clusters on HOPG are not known.

Recently we have carried out a core level photoemission and photoabsorption experiment for different Si thin films deposited on Highly Oriented Pyrolitic Graphite (HOPG) and insulating Sapphire (Al_2O_3). The in-situ measurements were performed at BL27A, Photon Factory. Si was deposited on the substrates at room temperature by using electron deposition method. After Si deposition, sample was transferred to analysis chamber, and Si 1s photoemission spectra and photoabsorption spectra at Si 1s near edge were measured.

In Figs. 1(a), 1(b) and 1(c), several Si 1s photoemission spectra are shown. The excitation energy was hν =2.2 keV. Figures 1(a) and 1 (b) show spectra for Si films on HOPG. The thicknesses of Si films are 0.3 Å and 5.5 Å, respectively.

In Fig. 1(b), there is only one component, "A". However, in the case of thinner film, i.e., 0.3 Å film in Fig. 1(a), there are more three components along with component "A". The relative binding energies for four components (A, B, C and D) are 0, 1.45, 2.85 and 4.25 eV, respectively.

The presence of several components in the photoemission spectra confirms the existence of a range of Si morphologies consisting of clusters and nanowires. Compared with other films, such as 0.4 Å, 2.3 Å and 4.5 Å, we identified two relatively stable Si phases corresponding to components "A" and "C". The binding energy difference between A and C is about 2.85 eV. Comparing with a previous result [3], we describe the component "C" originates from a cluster forming with an average of 10 Si atoms. According to Ref. 1, we predict that this 10-atom Si-clusters is polymerized, and become Si nanowires. At further deposition, the bulk-like component (A) starts to dominate, and finally remains for thicker films. Similar with thin Si on HOPG, thin Si on Sapphire in Fig. 1(c) also shows four different components, and their relative binding energy positions are also same to Si/HOPG. However, component C is more intense than others. From this photoemission measurement, it is understood that the morphology of Si corresponding to component "C" is a stable when Si is very thin grown on both HOPG and Sapphire.

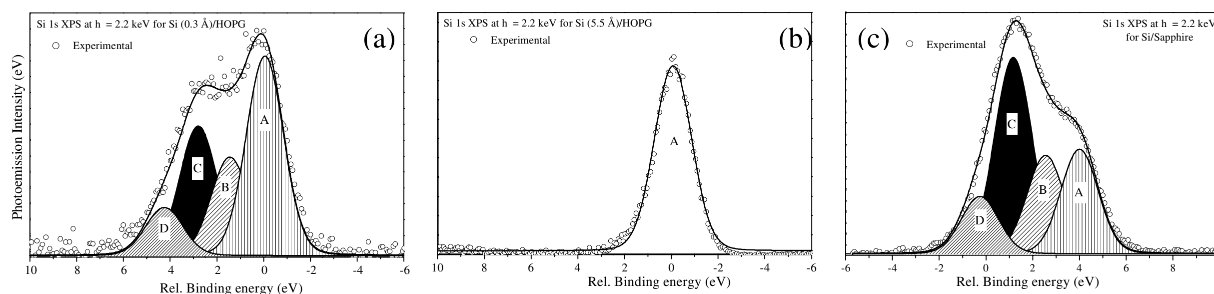

Figure 1. (a) Si1s photoemission spectra for a thin Si on HOPG. Four peaks are fitted to the experimental spectrum. (b) Si1s photoemission spectrum for thicker Si film on HOPG. Only a single component is observed. (c) Si1s photoemission spectra for a thin Si on Sapphire. Similar with thin Si on HOPG, four components are found.

[1] B. Marsen and K. Sattler, Phys. Rev. B, **60**, 11593 (1999), [2] S. Cristoloveanu, Solid-State Electronics **45**, 1403 (2001), [3] K. Fuke, et al., J. Chem. Phys. **99**, 7807 (1993).

*krishna@popsvr.tokai.jaeri.go.jp

27A/2001G334

XPS and NEXAFS observations on Si_xC produced by ion implantation

Yuji BABA*, Iwao SHIMOYAMA, Tetsuhiro SEKIGUCHI, Krishna G. NATH
Japan Atomic Energy Research Institute, Tokai-mura, Naka-gun, Ibaraki-ken 319-1195, Japan

Introduction

Recent rapid progress in semiconductor technology is accelerating the search for new two-dimensional (2D) semiconductor materials. Silicon carbide, one of the well-investigated semiconductors, tends to form three-dimensionally spread lattice with sp^3 bond. However, the recent theoretical study on 2D layer of SiC has revealed that the exactly flat 2D-SiC layer with graphite-like structure possibly exists [1]. In order to confirm the existence of such 2D-SiC, we have investigated the local electronic and geometric structures of Si^+-ion implanted graphite (HOPG). In the previous report, we showed that the NEXAFS spectra at the Si *K*-edge for Si^+-implanted HOPG has polarization dependence [2]. Here we report the X-ray photoelectron spectroscopic as well as NEXAFS spectroscopic observations on this system, and show the geometric structure of the Si-C bonds.

Experimental

The experiments were performed at the BL-27A station. The synchrotron beam was linearly polarized in horizontal direction. Atomic Si^+ ions were bombarded on HOPG single crystal from surface normal up to 1.4×10^{15} atoms/cm^2. For comparison, diamond-like carbon (DLC) without orientation was also used as substrate. The Si 1s-XPS was taken with hemispherical electron energy analyzer (VSW Class-100) using 2100 eV photons. The NEXAFS spectra were taken by the total electron yields.

Results and discussion

Figure 1 shows the XPS spectra around the Si 1s region excited by 2100-eV photons. The surface C/Si ratios of the Si^+-ion bombarded HOPG and DLC were estimated to be 0.01 on the basis of the C 1s/Si 1s peak intensity ratios. The binding energy of the Si 1s for Si^+-ion implanted DLC is almost the same as that for the SiC, suggesting that the amorphous Si_xC composed of sp^3 bonds is formed. While the Si 1s peak for Si^+-ion implanted HOPG shifts to higher binding energy by 1.3 eV than that for SiC, which suggests that the Si^+-ion implanted HOPG forms new layer where carbon atoms are more negatively charged than those in normal SiC.

Figure 2 displays the polarization dependence of the Si *K*-edge NEXAFS spectra for the Si^+-ion implanted HOPG (a) and DLC (b) at a fluence of 7×10^{13} atoms/cm^2. For Si^+-ion implanted HOPG, remarkable polarization dependence is observed for the peak A. The intensity of the peak A increases with the decrease in the incident angles of the synchrotron beam. On the other hand, no polarization dependence is observed in the spectra for Si^+-ion implanted DLC.

Considering the polarization dependence of peak A in fig.2(a), it is elucidated that the final state orbitals represented by the peak A are perpendicular to the basal plane of graphite sheet, i.e., parallel to the c-axis of graphite Thus it is presumed that some of the carbon atoms in graphite are substituted by the implanted silicon atoms, and the Si-C σ-bond thus produced is nearly parallel to the basal plane of the graphite sheet. The present results reveal that the two-dimensional Si_xC layer surely exists at low Si concentration.

References

[1] M. Fuentes-Cabrera et al., Model. Simul. Mater. Sci. Eng. **7**, 929 (1999).
[2] Y. Baba et al. Photon Factory Activity Report 2000 18 (2001).

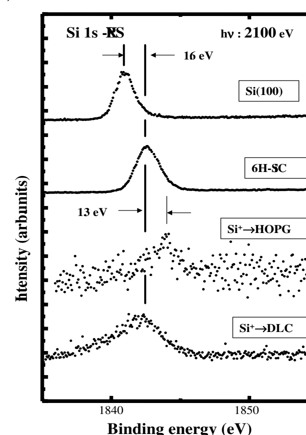

Fig.1 X-ray photoelectron spectra around Si 1s region excited by 2100-eV photons.

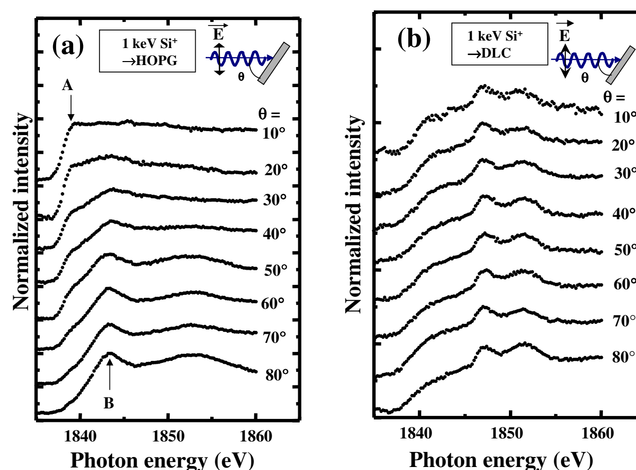

Fig.2 Polarization dependencies of Si *K*-edge NEXAFS spectra for (a) Si^+-ion implanted HOPG, and (b) Si^+-ion implanted DLC.

*ybaba@popsvr.takai.jaeri.go.jp

11B/2001G336

Metal induced gap states at LiCl/Cu(001) interface studied by x-ray absorption fine structure

Manabu KIGUCHI*[1], Genki YOSHIKAWA[2], Masao KATAYAMA[2], Koichiro SAIKI[1], Atsushi KOMA[2]
[1] Graduate School of Frontier Sciences, The University of Tokyo, Bunkyo, Tokyo 113-0033, Japan
[2]Graduate School of Science, The University of Tokyo, Bunkyo-ku, Tokyo 113-0033, Japan

Introduction

There has been a growing interest in metal/insulator systems due to their importance in catalysis, device applications and fundamental science. However, the large difference in chemical bond between metals and insulators makes it difficult to form an well-ordered interface. Recently, we could reveal that some alkali halide film grow heteroepitaxially on metal surfaces in a layer-by-layer fashion. In the present study, the electronic structures of LiCl/Cu(001) and LiCl/Ag(001) have been studied using NEXAFS, as a model system of the metal/insulator (alkali halide) interface.

Experiment

A mechanically and electrochemically polished Cu(001) and Ag(001) crystals were cleaned by repeated cycles of Ar^+ sputtering and annealing at 900 K. LiCl was evaporated from a Knudsen cell. Cl-*K* edge NEXAFS measurements were carried out at the soft x-ray double-crystal monochromator station BL-11B of the Photon Factory in National Laboratory for High Energy Physics.

Results and Discussion

Figure 1 shows the thickness and polarization dependence of the Cl K-edge NEXAFS for LiCl film grown on Cu(001). A well-pronounced pre-peak (peak 1) was observed on the bulk edge onset for the thin LiCl film grown on Cu(001). The intensity of the pre-peak increased with a decrease in film thickness. The pre-peak extended approximately 4 eV on the low energy side. The pre-peak was also observed for LiCl/Ag(001). LiCl grows on Cu(001) with its [100] axis rotated by 45° from that of the metal substrate ($[100]_{film}//[110]_{substrate}$), while LiCl grows on Ag(001) without azimuthal rotation ($[100]_{film}//[100]_{substrate}$). The pre-peak was observed irrespective of the interface structure. The energy of Cu MMM AES for LiCl/Cu(001) was the same as that for Cu(001) within 0.1 eV, indicating that Cu-Cl bond was not formed at the interface. Furthermore, the Cl 1s XPS results shows that only Li-Cl bond was formed for LiCl/Cu(001), since there is no sub-peak. These experimental results indicate that the pre-peak did not derive from the local Cu-Cl bond at the interface. The Cl-*K* edge pre-peak, and the gap state which they reflected, could be qualitatively understood as metal-induced gap state (MIGS). The MIGS were first introduced for semiconductor/metal junctions, but are also applicable to insulator/metal interfaces, such as MgO/Cu. In the present study, we could observe the MIGS for alkali halide/metal interfaces. The MIGS are the tails of the metal wave functions that decay exponentially into the insulating side of the interface. Next, we would discuss the character of MIGS formed at LiCl/Cu(001) interface. The MIGS peak was most enhanced at grazing x-ray incidence, implying that MIGS spread toward the surface normal direction. By analyzing the thickness dependence of the intensity of pre-peak, the decay length(ˇ) of MIGS was determined to be 0.2 nm. The decay length is shorter for states that are farther in energy from the band edge, that is, ˇ decreases with the band gap. For Si/Cu interface, the band gap of Si is 1.2 eV and ˇ is 0.6 nm. On the other hand, the band gap of LiCl is as large as 9.4 eV, it is, thus, natural that ˇ is 0.2 nm for LiCl/Cu.

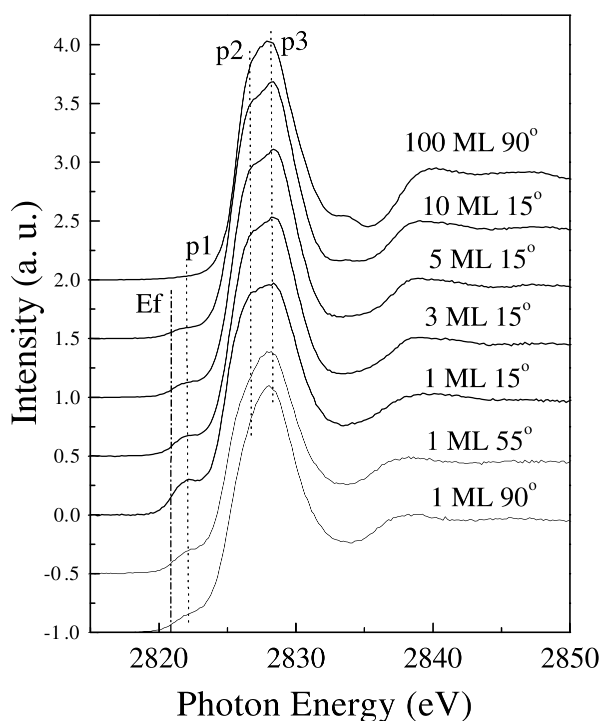

Fig. 1: Thickness and polarization dependence of the Cl K-edge NEXAFS for LiCl film grown on Cu(001).

* kiguchi@k.u-tokyo.ac.jp

10B/2001P016

Structures of low-dimensional ionic solutions confined in solid nanospaces

Takahiro OHKUBO[1], Yoshiyuki HATTORI[2], Hirofumi KANOH[1, 2], Katsumi KANEKO*[1, 2]
[1]Material Science, Graduate School of Science and Technology
[2]Center for Frontier Electronics and Photonics
Chiba University, 1-33 Yayoi, Inage, Chiba 263-8522, Japan

Introduction

It is well known that molecules form an ordered structure in solid nanospaces.[1, 2] Ionic solutions have been interested in a variety of fields in physics and chemistry. The structures of electrolytes have been studied actively. The characterization of electrolytes confined in nanospace is also important from aspects of development of industrial materials such as supercapacitor. An explicit anomaly in the hydration structure of rubidium bromide solution confined in the slit-shaped carbon nanospaces of the slit-width of about 1 nm is described in this report.

Experimental

Pitch-based activated carbon fiber (ACF, AD'ALL Co. Ltd.) was used as a nanoporous carbon having nano-scale slit-shaped space whose width was evaluated to be 1.1 nm from the nitrogen adsorption isotherm and subtracting pore effect (SPE) method. RbBr "nanosolution" confined in nanospaces of ACF was prepared by dissolution of deposited RbBr in adsorbed water. ACF having "nanosolutions" of 0.1 or 1 M RbBr were sealed in glass cell with Lumirror film (350 µm: Toray Ind. Inc.) All EXAFS spectra were recorded at BL-10B of Photon Factory, High Energy Accelerator Research Organization in Tsukuba.

Results and Discussion

Figures 1 and 2 show the Fourier transform of Rb and Br K-edge of RbBr "nanosolution" confined in ACF. The peak positions stemming from the 1st hydration shell around Rb and Br ions were similar to those of bulk aqueous solution of 1 M. The results with FEFF procedure are shown in Table 1. We used the hydration model of 2.8 Å for Rb-O distance and 3.3 Å for Br-O distance, respectively. The coordination number and Debye-Waller factor around both Rb and Br ions were decreased compared with those of bulk RbBr aqueous solution. These results indicate that dehydration of water molecule around both cation and anion confined in carbon nanospace is induced and cluster formation of water molecule is enhanced. This coincides that water molecules confined in hydrophobic micropores could form highly ordered structure even at 303 K.[1] Therefore, the dehydration effect in hydrophobic nanospace should be the result of strong ordering of water molecules in nanospace.

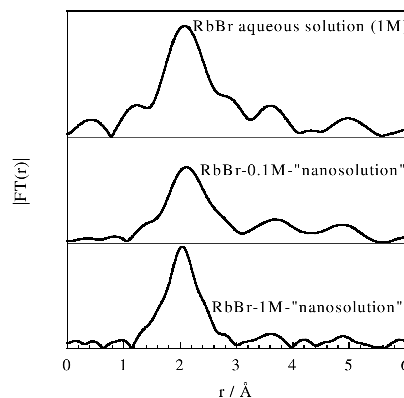

Fig. 1 Fourier transforms of Rb K-edge EXAFS of RbBr "nanosolution" and aqueous solution of 1 M.

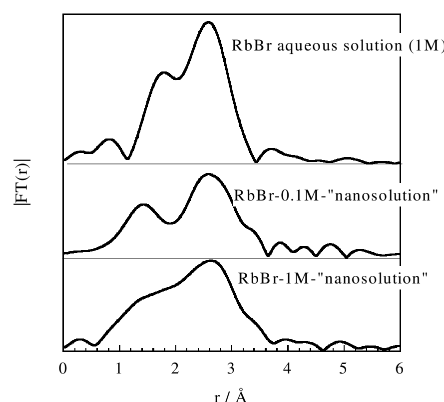

Fig. 2 Fourier transforms of Br K-edge EXAFS of RbBr "nanosolution" and aqueous solution of 1 M.

TABLE 1. EXAFS parameters from curve-fitting.

Sample	RbBr-1M-nanosolution	RbBr-0.1M-nanosolution	RbBr solution (1M)
$r_{Rb\text{-}O}$ (Å)	2.81	2.82	2.83
$r_{Br\text{-}O}$ (Å)	3.23	3.29	3.25
$N_{Rb\text{-}O}$	5.1	2.3	6
$N_{Br\text{-}O}$	2.4	1.3	6
$\sigma_{Rb\text{-}O}$ (Å)	0.070	0.069	0.111
$\sigma_{Br\text{-}O}$ (Å)	0.182	0.121	0.197

References

[1] T. Iiyama *et al.*, *J. Phys. Chem.*, **99**, 10075 (1995).
[2] T. Ohkubo *et al.*, *J. Phys. Chem. B*, **103**, 1859 (1999).
*ohkubo@pchem2.s.chiba-u.ac.jp

7A/2001S2-003

In-situ observation of water formation reaction on Pt(111) with dispersive NEXAFS

Masanari NAGASAKA[1], Hiroshi KONDOH[1], Kenta AMEMIYA[1], Akira NAMBU[1], Toru SHIMADA[1], Ikuyo NAKAI[1], and Toshiaki OHTA[*1]
[1]Department of Chemistry, Graduate School of Science, The University of Tokyo, Tokyo, Tokyo 113-0033, Japan

Introduction

The catalytic formation of water from adsorbed oxygen and hydrogen atoms on Pt(111) has been extensively studied because it is one of the simplest model reactions to understand the mechanisms of heterogeneous catalyses at the atomic level. Although a recent STM study [1] has provided a deep insight into the reaction mechanism, there still remains open questions, particularly about behaviour of an intermediate species (OH). This is because STM observations give only information on a local area of a microscopic scale, while the two-dimensional distribution of the intermediate species rapidly propagates in a mesoscopic scale. It is essential for the understanding of this reaction to observe real-time change of the reaction species on the whole surface. Dispersive NEXAFS [2] is a powerful tool to conduct the observations of the reaction with spectroscopic approach. Here we report preliminary results of dispersive NEXAFS measurements for the water formation reaction on Pt(111).

Experimental

The experiments were performed at BL-7A using an ultrahigh vacuum system (2.0×10^{-10} Torr). This system is equipped with a position-sensitive electron energy analyzer which is used for detecting Auger electrons emitted from the surface. Since the sample surface was irradiated by energy dispersed x rays, the position-sensitive detection of the Auger electrons provides a NEXAFS spectrum by Auger electron yield in a one-shot manner. It takes usually 40 sec to obtain a spectrum with reasonably high signal-to-noise ratio.

The Pt(111) surface was pre-covered by a p(2x2) layer of atomic oxygen. This surface was exposed to gaseous hydrogen ($0.1\text{-}1.0\times10^{-8}$ Torr) at a typical surface temperature of 130 K, where no water desorption takes place. Dispersive O K-edge NEXAFS spectra were taken during hydrogen exposure.

We also measured NEXAFS spectra of an OH-covered Pt(111) surface by the conventional partial-electron-yield method as the standard. The OH-covered surface was prepared by dosing H_2O on (2×2)-O/Pt(111) at 135 K and subsequent annealing at 175 K.

Results and discussion

Typical results of dispersive-NEXAFS measurements at normal incidence are shown in Fig.1. Although it is obviously recognized that a peak due to atomic oxygen (530 eV) disappears and a broad structure mainly associated with water (540 eV) increases with exposure, no OH-induced peak appears during the reaction. The absence of OH feature is due to a small transition probability of the OH species for the normal-incidence spectra at the low-energy region as shown in Fig. 2. The OH species gives a strong peak at 531 eV in the grazing-incidence spectrum. Therefore we measured dispersive NEXAFS at grazing incidence and found a component that is ascribed to the OH species after properly subtracting the atomic-oxygen component. Time-dependent change of the surface O, OH and H_2O species during the water-formation reaction has been thus obtained and kinetic analyses for the data are now underway.

References

[1] S. Völkening et al., Phys. Rev. Lett. 83, 2672 (1999).
[2] K. Amemiya et al., Jpn. J. Appl. Phys. 40, L718(2001)

*ohta@chem.s.u-tokyo.ac.jp

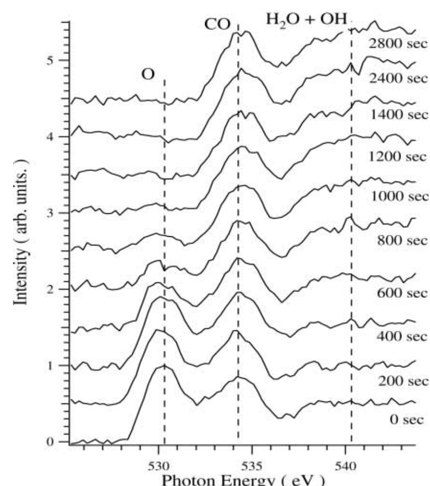

Fig. 1. Dispersive NEXAFS at normal incidence (150 K, hydrogen pressure 8.0×10^{-9} Torr).

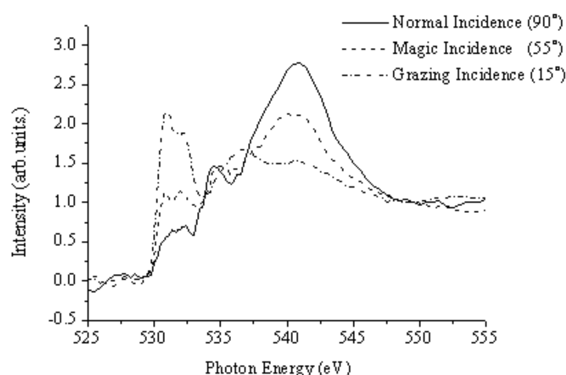

Fig.2 . NEXAFS of OH – Pt(111) at 150 K

7A/2001S2-003

The mechanism of CO oxidation on Pt(111) surface studied by energy-dispersive NEXAFS

Ikuyo NAKAI, Hiroshi KONDOH*, Kenta AMEMIYA, Akira NAMBU, Toru SHIMADA,
Masanari NAGASAKA and Toshiaki OHTA
Department of Chemistry, Graduate School of Science, The University of Tokyo, Hongo, Tokyo 113-0033, Japan

Introduction

CO oxidation on Pt(111) surface is a prototypical heterogeneous catalytic reaction and has been extensively studied by various methods. A previous STM study [1] showed that when two-dimensional islands of atomic oxygen on Pt(111) surface are exposed to gaseous CO molecules, oxidation proceeds exclusively at island perimeters after a certain "induction time". No reaction takes place during it.

Recently we developed a new technique, energy dispersive near edge x-ray absorption fine structure (NEXAFS) [2]. By using dispersed soft x-ray and position sensitive electron analyzer (GAMMADATA-SCIENTA, SES-2002), an Auger electron yield NEXAFS spectrum is obtained in one shot. We applied this new technique to monitor CO oxidation on Pt(111) and reconsidered its kinetics and reaction mechanism by a spectroscopic approach.

Experimental

The O *K*-edge energy-dispersive NEXAFS spectra were taken at BL-7A by the method described above.

Initially we prepared a Pt(111) surface covered with islands of atomic oxygen. Then the substrate was exposed to gaseous CO with a constant pressure at a constant substrate temperature. O-*K* dispersive NEXAFS spectra were taken in every forty seconds during CO exposure.

Results and discussion

Fig. 1 is a typical series of O-*K* dispersive NEXAFS during the reaction. The initial oxygen layer was annealed at 240 K and $1x10^{-8}$ Torr of CO gas was introduced at 240 K. Two peaks corresponding to CO π^* and atomic oxygen are observed. The latter continuously decreases as the reaction proceeds. CO_2 molecules desorb directly upon formation. Fig.2 shows time evolution of the coverage of O and CO evaluated by curve fitting for each spectrum in Fig. 1. Apparently no "induction time" is observed and the coverage of atomic oxygen falls immediately as adsorption of CO starts in contrast to the previous observation by STM [1]. The curve for the reduction of atomic oxygen is classified into two processes at about 300 second. Oxygen reduces faster in the first process. Detailed analysis of the reaction rate revealed that the reaction rate in the first process is proportional to the coverage of atomic oxygen and that in the second process is proportional to its square root. This kinetic order for the second process suggests that the reaction takes place at island perimeters in accordance with the result of the STM study [1]. The first process probably takes place during the induction time for the second one.

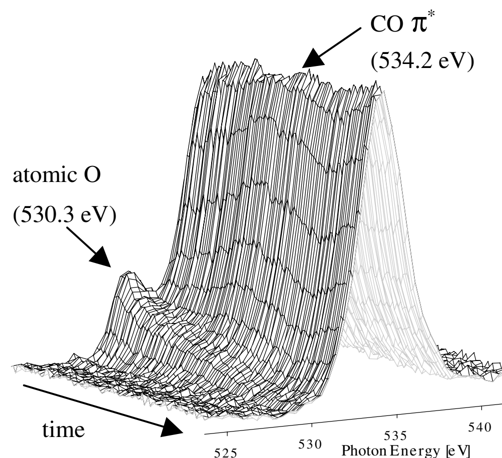

Fig. 1: Series of O-*K* energy-dispersive NEXAFS during the reaction of CO+O/Pt(111) at 240 K

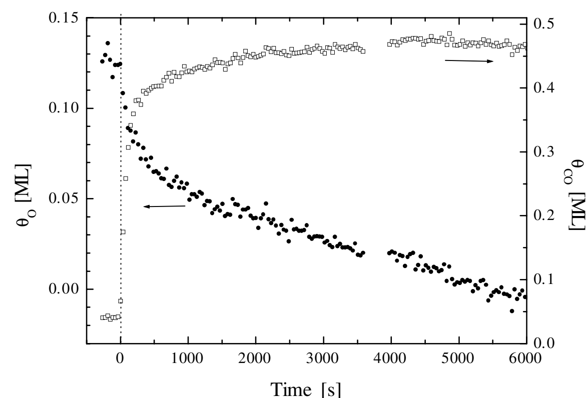

Fig. 2: Time evolution of coverage of O and CO obtained from the result of Fig. 1

An oxygen-covered surface annealed at higher temperature is expected to be more highly ordered. When we started a reaction for an oxygen-covered surface preannealed at a higher temperature, less amount of oxygen reacted in the first process. This suggests that the first process is associated with disordered atomic oxygen. We consider that oxygen atoms diffusing between immobile islands react in the first process faster than ones in islands and that because of their high mobility such a reaction process was undetectable with STM.

References

[1] J. Wintterlin et al., *Science* **278**, 1931 (1997).
[2] K. Amemiya et al., *Jpn. J. Appl. Phys.* **40**, L718 (2001).

*kondo@chem.s.u-tokyo.ac.jp